energies

MDPI

Article

Characteristics and Controlling Factors of Natural Fractures in Lacustrine Mixed Shale Oil Reservoirs: The Upper Member of the Lower Ganchaigou Formation in the Ganchaigou Area, Qaidam Basin, Western China

Xing Zhao [1,2,*], Guiwen Wang [1,2,*], Dong Li [1,2], Song Wang [1,2], Quanwei Sun [1,2], Jin Lai [1,2], Zongyan Han [1,2], Yafeng Li [3], Yinghao Shen [1] and Kunyu Wu [3]

[1] State Key Laboratory of Petroleum Resources and Engineering, China University of Petroleum (Beijing), Beijing 102249, China
[2] College of Geosciences, China University of Petroleum (Beijing), Beijing 102249, China
[3] Research Institute of Petroleum Exploration and Development, Qinghai Oilfield Company, CNPC, Dunhuang 736202, China
* Correspondence: zhaox0402@163.com (X.Z.); wanggw@cup.edu.cn (G.W.)

Abstract: Natural fractures within the lacustrine mixed shale oil reservoirs of the upper member of the Lower Ganchaigou Formation (E_3^2) in the Ganchaigou area of the Qaidam Basin are pivotal to the exploration and development of shale oil and gas. This research investigates the developmental characteristics and controlling factors of natural fractures and their impact on the reservoir quality based on cores, image logs, thin sections, scanning electron microscopy observations, and experimental and production data. The results indicate that natural fractures in the E_3^2 are categorized into tectonic fractures, diagenetic fractures, and abnormal high-pressure fractures. Tectonic fractures are characterized by a significant variation in dip angles, a wide range of apertures, low density, and a high filling degree. Diagenetic fractures typically exhibit low dip angles, small apertures, high density, and a low filling degree. Abnormal high-pressure fractures display chaotic orientations and complex styles, often consisting of filled fractures. The development and distribution of natural fractures are jointly influenced by mineral composition and brittleness, lamination structure, organic matter content and maturity, diagenesis, tectonic factors, and abnormal high pressure. A high content of dolomite, thin-bedded structures comprising carbonate laminae and felsic laminae, and abundant mature organic matter provide a favorable foundation for fracture development. Diagenesis, including dissolution, pressure solution, and mineral dehydration shrinkage, acts as a beneficial guarantee for fracture development. Tectonic locations near the hanging wall of faults and the core of anticlines are the main regions for fracture development. Abnormal high pressure is a crucial driving force for fracture development. Interconnected natural fractures of various types and scales significantly expand reservoir space and enhance pore connectivity and flow capacity, serving a vital function in maintaining high and stable production in lacustrine mixed shale oil reservoirs.

Keywords: lacustrine mixed shale oil reservoirs; natural fractures; characteristics; controlling factors; the upper member of the Lower Ganchaigou Formation

check for updates

Citation: Zhao, X.; Wang, G.; Li, D.; Wang, S.; Sun, Q.; Lai, J.; Han, Z.; Li, Y.; Shen, Y.; Wu, K. Characteristics and Controlling Factors of Natural Fractures in Lacustrine Mixed Shale Oil Reservoirs: The Upper Member of the Lower Ganchaigou Formation in the Ganchaigou Area, Qaidam Basin, Western China. *Energies* **2024**, *17*, 5996. https://doi.org/10.3390/en17235996

Academic Editor: Dameng Liu

Received: 1 November 2024
Revised: 23 November 2024
Accepted: 25 November 2024
Published: 28 November 2024

Copyright: © 2024 by the authors. Licensee MDPI, Basel, Switzerland. This article is an open access article distributed under the terms and conditions of the Creative Commons Attribution (CC BY) license (https://creativecommons.org/licenses/by/4.0/).

1. Introduction

Global hydrocarbon reserves have witnessed substantial growth, driven by the rapid advancement and effective exploitation of shale oil and gas resources [1–5]. The remarkable success of shale oil exploration and development in the United States has reshaped the global energy supply–demand landscape [3–5]. In China, shale oil resources are primarily distributed in continental lacustrine basins [6,7]. Among these, lacustrine mixed shale oil reservoirs have become a key exploration focus due to their considerable hydrocarbon generation potential and complex geological characteristics [8–10]. These reservoirs mainly

comprise fine-grained mixed sedimentary rocks with poor matrix porosity and permeability [11,12]. However, owing to their diverse mineral composition, intricate interbedded laminations, and pronounced heterogeneity, these reservoirs are prone to developing various types of natural fractures influenced by diagenetic and tectonic processes [13,14]. Natural fractures significantly improve the physical properties of shale oil reservoirs, influencing the migration and accumulation of hydrocarbons [14–16]. Furthermore, during hydraulic fracturing, natural fractures play a crucial role in altering the propagation and distribution of hydraulic fracture networks [17,18]. Therefore, comprehensive research into natural fractures in lacustrine mixed shale oil reservoirs is essential for identifying sweet spots and optimizing development strategies.

Extensive research has been conducted on the characteristics [19–21], formation mechanisms [22–24], and the identification and characterization methods of natural fractures in hydrocarbon reservoirs [25–27], leading to numerous breakthroughs, particularly in tight sandstone reservoirs [28,29], carbonate reservoirs [21,24,26], and marine shale reservoirs [15,23,30]. Compared to these reservoirs, lacustrine mixed shale oil reservoirs present greater complexity due to their highly variable depositional environments, mixed sedimentary minerals, frequent interbedded laminations, and intricate diagenetic evolution [31–33]. Consequently, the development of natural fractures in lacustrine mixed shale oil reservoirs exhibits unique and complex characteristics [15,34]. However, current research on natural fractures within lacustrine shale oil reservoirs remains limited, with even fewer studies focusing specifically on lacustrine mixed shale oil reservoirs [13,35,36]. This gap has resulted in an insufficient understanding of the characteristics, controlling factors, and formation mechanisms of natural fractures in these reservoirs, which in turn constrains effective exploration and economic development.

This study investigates natural fractures in lacustrine mixed shale oil reservoirs mainly from macroscopic and microscopic perspectives, utilizing data from cores, thin sections, scanning electron microscopy observations, X-ray diffraction analysis, organic geochemical analysis, and image logs of the upper member of the Lower Ganchaigou Formation in the Ganchagou area of the Qaidam Basin. This study aims to (1) determine the types and characteristics of natural fractures in lacustrine mixed shale oil reservoirs; (2) analyze the key controlling factors of natural fracture development in lacustrine mixed shale oil reservoirs; and (3) discuss the impact of natural fractures on reservoir quality and hydrocarbon production in lacustrine mixed shale oil reservoirs.

2. Geological Setting

The Qaidam Basin, located in the northern part of the Tibetan Plateau, is the only large continental hydrocarbon-bearing basin in Western China predominantly composed of Cenozoic strata (Figure 1A) [9]. The isolation provided by the Altun, Kunlun, and Qilian mountain ranges have resulted in the region's arid climate and complex geographical environment [37,38]. The basin has an average elevation of 2900 m and covers an area of approximately 1.2×10^5 km^2, exhibiting an irregular rhomboid shape that is wider in the west and narrower in the east [9,38]. Based on the basin's tectonic structure and geophysical characteristics, it can be divided into three primary structural units, namely Western Qaidam Depression, Northern Qaidam Fault Depression, and Sanhu Depression [9]. The Yingxiongling structural belt is situated within the Western Qaidam Depression and is a tectonic uplift zone formed during the late Himalayan orogeny, characterized by various folds, detachment deformations, and fault structures (Figure 1B) [39]. Since the Cenozoic, the area has undergone three tectonic evolution stages. Which are the Paleogene fault depression, the early Miocene to early Pliocene weak compression, and the late Pliocene to Quaternary strong compression phases [39]. Influenced by the left lateral strike-slip faults of the East Kunlun and Altun Mountains, the Yingxiongling structural belt transitioned from an extensional stress regime in the Paleogene to a strike-slip compressional regime in the Neogene, resulting in a complex structural style [40]. The Ganchaigou block, serving as a pilot demonstration area and key breakthrough zone for Yingxiongling shale oil, is

located in the northwestern part of the Yingxiongling structural belt (Figure 1B). This area is characterized by a large nose-shaped slope that dips from the northwest to the southeast of the basin, exhibiting a relatively simple current structure [41]. Additionally, it displays a nearly rectangular planform with few developed faults (Figure 1C).

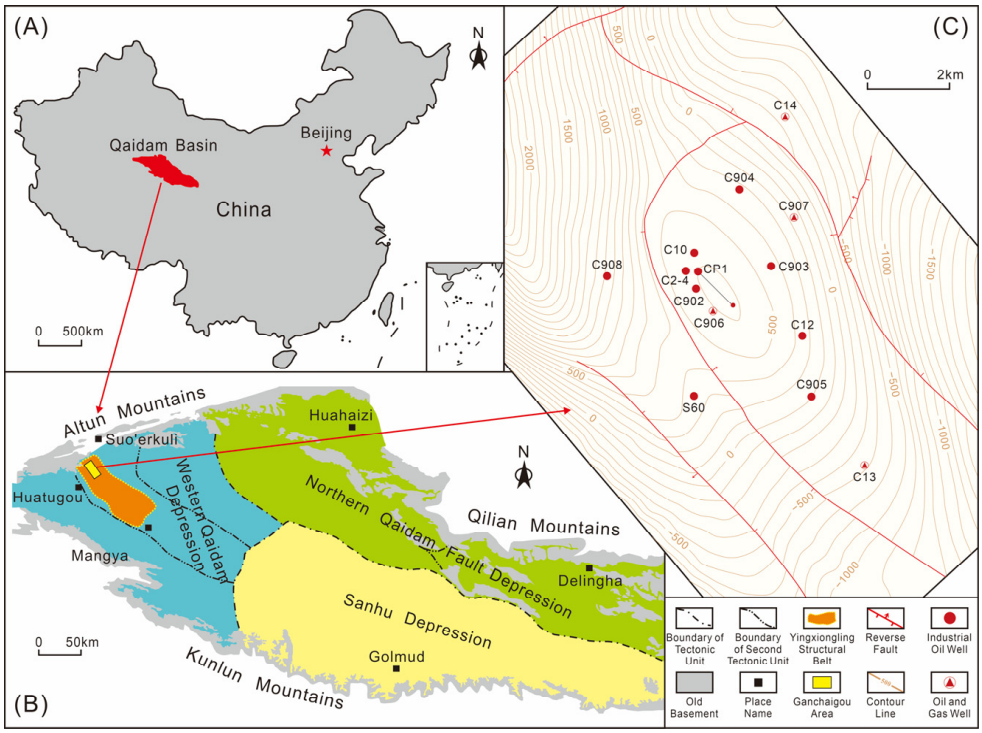

Figure 1. A regional index map showing the study area. (**A**) The location of Qaidam Basin in China. (**B**) A map showing the division of tectonic units in Qaidam Basin and the location of the Ganchaigou area in the Yingxiongling structural belt (modified from Li et al., 2022) [9]. (**C**) A structural map showing key well locations and major faults in the Ganchaigou area (modified from Guo et al., 2023) [41].

Under the control of the Altun, Qilian, and East Kunlun structural belts, the Qaidam Basin has deposited thick Mesozoic and Cenozoic strata [9]. The Ganchaigou area is primarily composed of Cenozoic strata, which from bottom to top include four stratigraphic units, namely the Lulehe Formation (E_{1+2}), the lower member of the Lower Ganchaigou Formation (E_3^1) and the upper member of the Lower Ganchaigou Formation (E_3^2), the Upper Ganchaigou Formation (N_1), and the Lower Youshashan Formation (N_2^1) [9]. The lacustrine mixed shale oil reservoirs are mainly developed in the E_3^2, which is divided into six oil layer groups from top to bottom. The upper section (oil layer group I–III) contains lime mudstone and gypsum-bearing mudstone interbedded with salt rock, with argillaceous calcareous dolomite and calcareous dolomite occurring at the top and bottom of the upper section, respectively. The lower section (oil layers IV–VI) is characterized by frequent alternations of argillaceous shale and calcareous dolomitic shale interspersed with calcareous dolomite and siltstone [9,42]. The overall thickness of the E_3^2 ranges from 1000 m to 2000 m, with the mixed shale series exceeding 1000 m in thickness [9], representing a significant proportion of the strata (Figure 2).

The formation and evolution of the Qaidam Basin is mainly divided into four stages. The Oligocene to Miocene period (E_3^1–N_1) represents the stage of lacustrine basin expansion and subsidence [43]. During this period, the basin was significantly influenced by seasonal rainfall, resulting in paleoclimatic fluctuations from arid to humid and back to arid during the E_3^2 depositional phase [44]. Correspondingly, the sedimentary environment transitioned through stages of semi-salinity, salinity, and ultimately to a salt lake [45]. In the early depositional stage (oil layer group VI), characterized as the semi-saline stage,

the basin experienced a large-scale transgression. The relatively warm and humid climate combined with suitable salinity promoted biological proliferation and growth within the basin, facilitating the accumulation and preservation of organic matter [9]. Concurrently, due to the combined effects of tectonic evolution and climatic changes, the basin's depocenter gradually shifted, with the Yingxiongling area becoming the sedimentary center of the Western Qaidam Depression [40]. This region saw an extensive deposition of mudstone and shale, establishing the foundation for the development of high-quality hydrocarbon source rocks in subsequent stages. In the mid-depositional stage (oil layer group V–IV), the basin entered the saline phase, characterized by a relatively cold and arid climate [9,42]. Sediment supplies diminished and intense evaporation led to an increased salinity in the lacustrine waters. In the late depositional stage (oil layer group III–I), the basin evolved into a salt lake. Influenced by global cooling, the climate became increasingly cold and arid, with a decreasing sediment supply, sustained evaporation, and a rapidly declining lake level causing the basin area to contract significantly [9,45]. Salinity levels rose markedly and an extensive development of gypsum and salt rocks occurred in the study area, creating favorable conditions for the accumulation and preservation of shale oil [42,45].

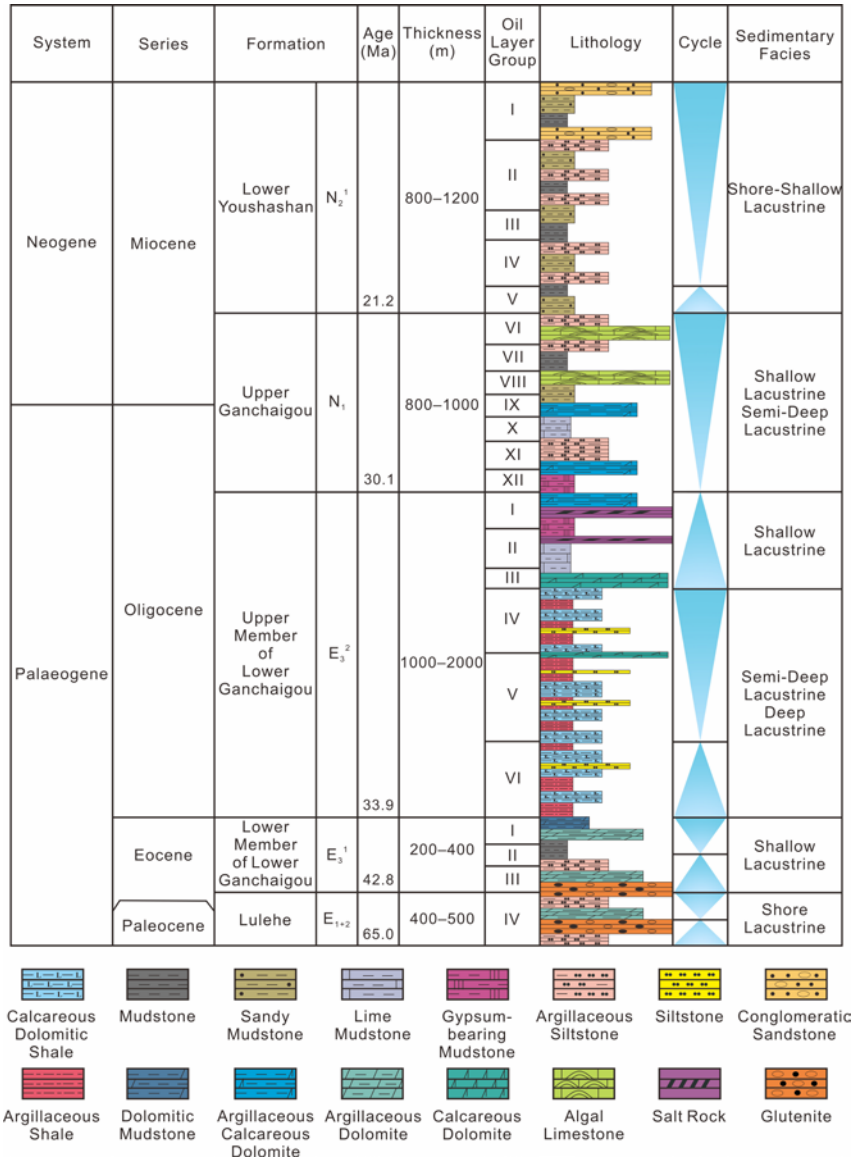

Figure 2. Sedimentary facies and stratigraphic column in the Ganchaigou area, Qaidam Basin (modified from Li et al., 2022) [9].

3. Data and Methods

The investigation and analysis of natural fractures in the upper member of the Lower Ganchaigou Formation, focusing on shale oil reservoirs, were conducted using cores, thin sections, scanning electron microscopy (SEM), borehole image logs, and related experimental data from 13 wells in the Ganchaigou area of Qaidam Basin. All wells investigated in this study were drilled vertically and are distributed across various structural positions (Figure 1C). A total of 381.43 m of core samples were obtained from seven cored wells (Figure 1C and Table 1). From these cores, 541 samples were selected to prepare thin sections (30 μm in thickness). Additionally, 48 samples were ion-polished with argon for field emission scanning electron microscopy (FE-SEM), and eight samples from well C2-4 were prepared for focused ion beam scanning electron microscopy (FIB-SEM) using freshly broken rock samples coated with a gold film on the surface. The experimental data include 228 X-ray diffraction (XRD) data records and 268 total organic carbon (TOC) data from well C908, 954 core porosity and permeability measurements from seven cored wells, and 20 vitrinite reflectance (Ro) measurements from well C906 and well S60. In addition, borehole image logs from Schlumberger's FMI imaging tool, covering a total length of 13167.40 m, were obtained from 11 wells in the Ganchaigou area (Table 1).

Table 1. Depth interval of the upper member of the Lower Ganchaigou Formation, cored interval, and borehole image interval of different wells in the Ganchaigou area, Qaidam Basin.

Well Number	Depth Interval of the Upper Member of the Lower Ganchaigou Formation	Cored Interval	Borehole Image Logs Interval
C2-4	2055.50–2883.00 m	2798.00–2851.00 m	2223.45–2897.00 m
C12	2297.00–3804.60 m	3520.00–3619.96 m	2447.70–3788.80 m
C13	2940.25–4722.00 m	3715.00–3733.10 m	3102.50–4723.00 m
		4215.00–4228.81 m	/
C14	2752.16–4527.45 m	3830.00–3866.00 m	3050.30–4522.45 m
C902	2048.20–3497.90 m	/	2651.00–3503.00 m
C903	2159.00–3512.50 m	/	2710.00–3505.80 m
C904	2253.00–3820.00 m	/	2413.00–3820.00 m
C905	2559.00–4070.00 m	/	2972.70–3405.00 m
C906	2087.50–3705.50 m	3225.00–3242.23 m	2779.50–3766.10 m
C907	2380.40–4106.30 m	/	2449.20–4185.60 m
C908	1728.00–3686.00 m	2750.00–2800.00 m	1992.00–3842.00 m
		3200.00–3281.30 m	/
S60	2538.00–4686.00 m	3025.64–3339.51 m	/
		3447.46–3456.70 m	/

"/" indicates no data available.

To characterize natural fractures at different scales, macroscopic and microscopic observations, descriptions, and analyses were performed. Macroscopic analysis was based on core samples and image log data. The image log data in the study area were acquired under water-based mud conditions. Prior to analysis, core samples were used to calibrate the image log data, ensuring depth consistency between the two datasets. After processing the image log data with speed correction, eccentering correction, and static and dynamic normalization, high-resolution color borehole images (with a vertical resolution of 5 mm) were generated to extract fracture attributes such as orientation, dip angle, density, and aperture. The processing and interpretation of image log data, as well as fracture parameter calculations, were conducted using the software Techlog 2019.2. Microscopic analysis involved the use of ordinary thin sections, cast thin sections, and SEM. Cast thin sections were injected with blue epoxy resin to highlight pores and microfractures. All thin sections were observed using a ZEISS Axio Imager 2 polarizing microscope (Carl Zeiss AG, Oberkochen, Germany) under both plane-polarized and cross-polarized light in accordance with the SY/T 5368-2016 standard [46]. FE-SEM images were captured using a Quanta

FEG-450 field emission scanning electron microscope (Thermo Fisher Scientific, Waltham, MA, USA), and FIB-SEM imaging was performed using a Zeiss Crossbeam 550 focused ion beam scanning electron microscope (Carl Zeiss AG, Oberkochen, Germany), both following the SY/T 5162-2021 standard [47].

Mineral XRD analysis was conducted using an Empyrean X-ray diffractometer (Malvern Panalytical, Almelo, The Netherlands). Prior to analysis, each sample was oven-dried at 105 °C for 2 h and then ground into fine powder (<2 μm) using a mortar and pestle. The entire experiment followed the SY/T 5163-2018 standard [48]. Core porosity was measured with the Ultra Pore-400 porosity meter (Porous Materials Inc., Ithaca, NY, USA), and permeability was measured using the Ultra Peam-410 permeability meter (Porous Materials Inc., Ithaca, NY, USA) with cylindrical plug samples of 25 mm in diameter. The entire process followed the GB/T 29172-2012 standard [49]. TOC measurements were performed using a CS230 carbon–sulfur analyzer (LECO Corporation, St. Joseph, MI, USA) according to the GB/T 19145-2022 standard [50]. This method involves the combustion of samples in a high-temperature oxygen stream, converting TOC into carbon dioxide. Prior to measurement, inorganic carbon was removed from the samples using dilute hydrochloric acid. Ro was measured using an MSP200 microspectrophotometer (J&M Analytik AG, Stuttgart, Germany). Samples were prepared as thin sections and stored in a desiccator for at least 12 h before measurement following the SY/T 5124-2012 standard [51], ensuring accuracy and reliability during the Ro analysis.

4. Results

4.1. Reservoir Characteristics

4.1.1. Petrological Characteristics

The XRD results indicate that the E_3^2 shale oil reservoirs are primarily composed of felsic minerals (quartz, potassium feldspar, and plagioclase feldspar), carbonate minerals (calcite, dolomite, and ankerite), and clay minerals (illite and illite/smectite mixed layer), along with minor amounts of anhydrite and pyrite. The mineral content varies frequently in the vertical profile (Figure 3A). Among them, carbonate minerals are the most abundant, ranging from 4.4% to 72.1% (average of 42.6%), clay minerals range from 9.7% to 47.3% (average of 26.3%), and felsic minerals range from 7.5% to 67.5% (average of 23.9%). The combined average of these three major mineral categories exceeds 90%, while pyrite and anhydrite each comprise less than 5% (Figure 3B).

Based on core samples, thin sections, and XRD results, the lithology of the study area can be categorized into argillaceous shale, calcareous dolomitic shale, calcareous dolomite, and siltstone. Argillaceous shale primarily appears charcoal gray in core samples, exhibiting well-developed laminae with a high density (Figure 4A). Microscopic analysis reveals two common types of lamina couplets (LCs). The first type comprises organic-rich clay laminae (OCL), calcite laminae (CAL) or dolomite laminae (DL), and quartz–feldspar–clay mixed laminae (QFCL) (Figure 4E). The second type consists of clay laminae (CL), QFCL, felsic mineral (quartz+feldspar) laminae (QFL), and felsic–carbonate–clay mixed laminae (QFCACL) (Figure 4H). In both cases, clay laminae are generally thicker than carbonate laminae. Calcareous dolomitic shale (or dolomitic calcareous shale) appears brown in core samples, characterized by frequent vertical color changes that correspond to variations in mineral composition, along with laminated structures (Figure 4B,C). Microscopic examination shows the LC comprises CL, QFCL, CAL, and quartz–feldspar–calcite mixed laminae (QFCAL) (Figure 4F). Another type of LC consists of CL, DL, and carbonate–clay mixed laminae (CACL) (Figure 4G). In these cases, carbonate laminae are generally thicker than clay laminae. Calcareous dolomite displays a taupe coloration in core samples and layered structures, characterized by a significantly lower frequency of vertical variations in color and mineral composition compared to shale (Figure 4D). Microscopic analysis reveals a mixture of abundant micritic calcite and micritic dolomite, along with minor clay and felsic minerals (Figure 4I). Siltstone is less developed, consisting of numerous felsic particles less

than 0.05 mm in size, primarily embedded in a matrix of mud and carbonate cement with dispersed pyrite observed between the particles (Figure 4J).

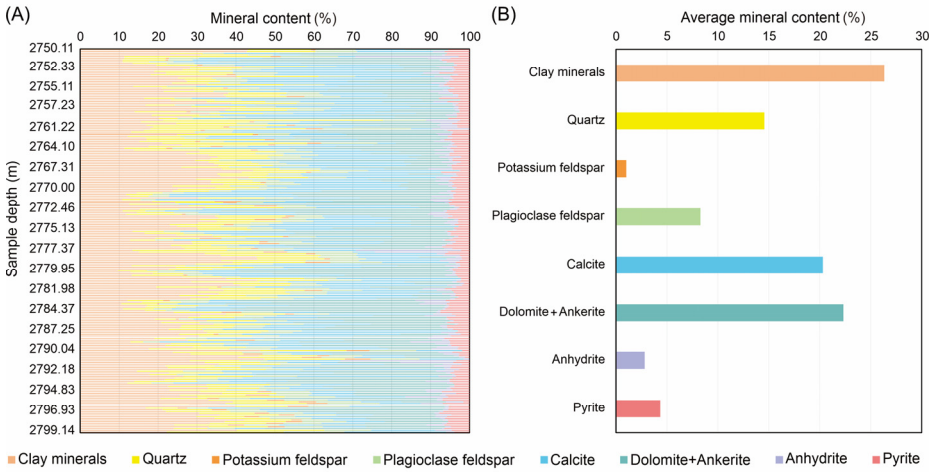

Figure 3. Mineral composition of the upper member of the Lower Ganchaigou Formation in the study area (well C908). (**A**) Mineral composition at different depths; (**B**) average content of minerals.

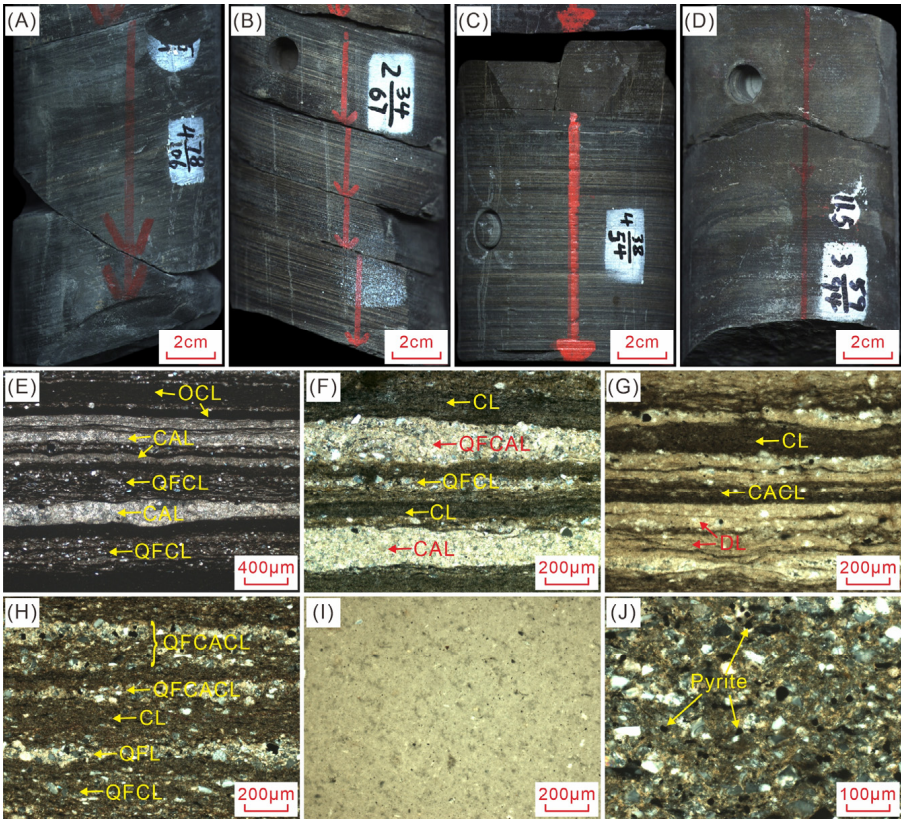

Figure 4. Petrological characteristics of shale oil reservoirs in upper member of Lower Ganchaigou Formation. (**A**) Argillaceous shale, well C908, 2796.47–2796.62 m, external surface of core; (**B**) calcareous dolomitic shale, well C13, 3725.67–3725.82 m, external surface of core; (**C**) dolomitic calcareous shale, well C2-4, 2822.08–2822.23 m, external surface of core; (**D**) calcareous dolomite, well C12, 3559.30–3559.45 m, external surface of core; (**E**) argillaceous shale, well C13, 3726.07 m, cross-polarized light; (**F**) dolomitic calcareous shale, well C2-4, 2844.47 m, cross-polarized light; (**G**) calcareous dolomitic shale, well C14, 3846.86 m, cross-polarized light; (**H**) argillaceous shale, well C12, 3600.78 m, cross-polarized light; (**I**) calcareous dolomite, well C908, 2772.46 m, cross-polarized light; (**J**) argillaceous siltstone, well C14, 3845.82 m, cross-polarized light.

4.1.2. Reservoir Space Types

Core, thin-section, and SEM observations indicate that the reservoir space in the study area includes intercrystalline pores, dissolution pores, organic matter pores, and fractures. Intercrystalline pores are further subdivided based on the host mineral into dolomite intercrystalline pores, pyrite intercrystalline pores, and clay mineral intercrystalline pores. Under the microscope, dolomite intercrystalline pores typically appear triangular, rhomboidal, or irregularly quadrilateral in shape, with small pore sizes primarily in the nanometer or submicron range. These pores are abundant and constitute the primary reservoir space in the study area (Figure 5A,B). Pyrite intercrystalline pores primarily develop within framboidal pyrite aggregates and exhibit irregular polygonal or lamellar shapes, with nanometer-scale pore sizes (Figure 5C). Clay mineral intercrystalline pores mainly develop within illite/smectite mixed layers and illite and are typically strip-shaped or slit-like, with nanometer-scale pore sizes (Figure 5D). Dissolution pores are predominantly intercrystalline dissolution pores, appearing elongated or honeycomb-like under a microscope, with irregular pore edges and micron-scale pore sizes (Figure 5E). Organic matter pores are rarely developed and are often associated with pyrite. Under a microscope, these pores appear near-circular, with nanometer-scale pore sizes (Figure 5F). In addition to matrix pores, fractures are also an important component of the reservoir space in the study area.

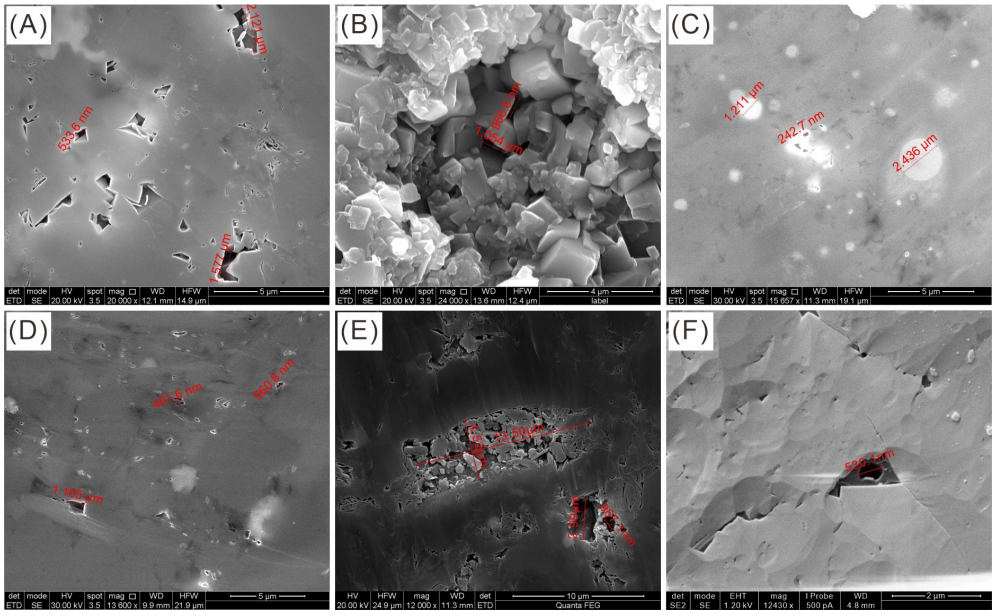

Figure 5. Scanning electron microscope (SEM) images show pore types in upper member of Lower Ganchaigou Formation. (**A**) Dolomite intercrystalline pores, well C2-4, 2817.18 m; (**B**) dolomite intercrystalline pores, well C906, 3229.29 m; (**C**) pyrite intercrystalline pores, well C14, 3831.82 m; (**D**) intercrystalline pores in clay minerals, well C14, 3845.61 m; (**E**) weak dissolution occurred along edges of intercrystal pores, well C908, 3275.91 m; (**F**) organic matter pores, well C2-4, 2822.69 m.

4.1.3. Reservoir Physical Properties

Core porosity and permeability measurements show that the reservoir porosity ranges from 0.02% to 15.38%, with an average of 3.36%. Permeability ranges from 0.01×10^{-3} μm^2 to 18.66×10^{-3} μm^2, with an average of 0.40×10^{-3} μm^2. The reservoir is characterized by ultra-low porosity and low permeability, and the correlation between porosity and permeability is weak (Figure 6). Notably, the porosity of samples without fractures exhibits a wider range and higher average values than those with fractures, while the permeability distribution shows the opposite trend.

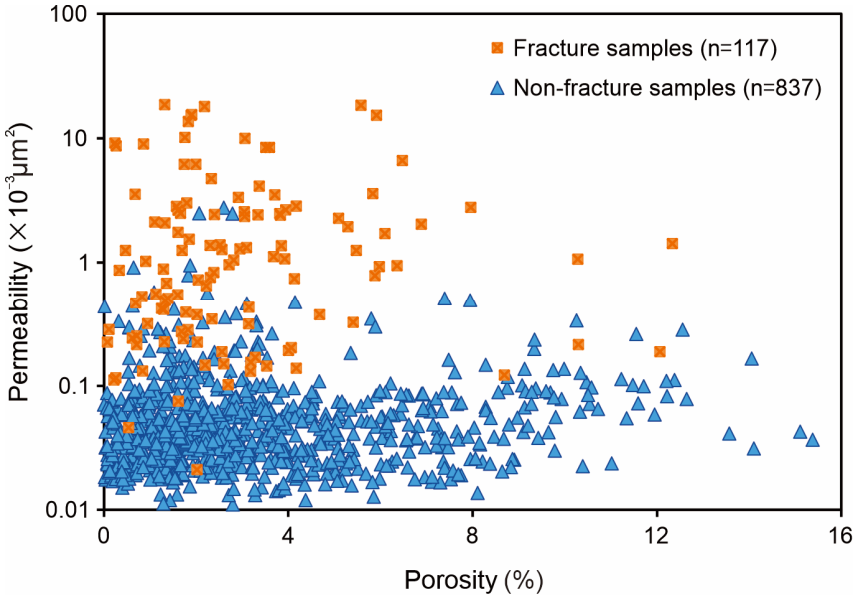

Figure 6. A cross-plot of porosity versus permeability for shale oil reservoirs in the upper member of the Lower Ganchaigou Formation.

4.2. Fracture Characteristics

4.2.1. Fracture Types

Natural fractures in the shale oil reservoirs of the E_3^2 in the Ganchaigou area are categorized into tectonic fractures, diagenetic fractures, and abnormal high-pressure fractures based on their geological origin, occurrence, mechanical properties, and observed characteristics in cores, thin sections, and SEM images. Tectonic fractures refer to discontinuous planar structures formed under tectonic deformation within the reservoir [52]. They are influenced by regional tectonic movements and stress fields, often characterized by variable orientations and uneven fracture apertures. Mechanically, tectonic fractures are further classified into shear fractures and tensile fractures. Diagenetic fractures arise during sedimentation and diagenesis due to diagenetic alterations [53]. They typically exhibit low dip angles, small apertures, and short extension lengths and are primarily categorized into bedding fractures, shrinkage fractures, and dissolution fractures in the study area. Abnormal high-pressure fractures occur when internal fluid pressure within the reservoir exceeds the rock's fracture pressure [53]. They display highly variable orientations, irregular shapes, and short extension lengths, with distinctive tensile characteristics. Additionally, fractures in the study area can be classified based on their dip angles into vertical fractures ($70° < \theta \leq 90°$), high-angle fractures ($45° < \theta \leq 70°$), low-angle fractures ($20° < \theta \leq 45°$), and horizontal fractures ($0° < \theta \leq 20°$). Additionally, fractures can be categorized according to their infilling conditions into filled fractures and unfilled fractures.

4.2.2. Macroscopic Fracture Characteristics

Natural fractures observed in core samples typically range from a millimeter to centimeter scale, providing a direct reflection of the macroscopic fracture characteristics in the study area. Observations indicate that shear fractures are extensively developed throughout the study region, representing a fracture type formed under shear tectonic forces. These fractures feature smooth and straight surfaces and extend for considerable distances, often cutting through entire core samples (Figure 7A). They exhibit a wide range of dip angles, with relatively narrow widths (Figure 7A,B,D). The degree of filling varies from unfilled to completely filled, with the primary filling material being anhydrite (Figure 7D). Tensional fractures are planar structures that arise from tensile forces acting on the reservoir. These fractures typically exhibit curved and rough surfaces and often display serrated extensions. They generally have shorter propagation distances and tend to develop at steep angles,

frequently approaching vertical orientations. The widths of fractures vary significantly, and they are commonly infilled with anhydrite and calcite (Figure 7C). Shrinkage fractures result from dewatering and shrinkage or recrystallization processes during the diagenesis of sediments [52]. They predominantly exhibit a V-shaped distribution in core samples, are generally small in scale, and have short extension distances with significant variations in aperture, often fully filled with calcite (Figure 7E). Dissolution fractures are formed due to the differential dissolution of reservoir minerals. These fractures exhibit considerable variability in scale, with inconsistent aperture widths and irregular edges, and they display unstable orientations. They are often filled with calcite (Figure 7F). Bedding fractures observed in core samples are aligned parallel or sub-parallel to bedding planes, with relatively small scales. They display straight surfaces, low dip angles, and mainly develop horizontally or at low angles (Figure 7G). Bedding fractures show relatively good continuity and are often observed to extend laterally, cutting across the core (Figure 7H). Most of these fractures are unfilled, with only a small portion being filled predominantly with calcite (Figure 7G). Abnormal high-pressure fractures result from rock failure under abnormal fluid pressure conditions. These fractures are characterized by irregular shapes, small scales, short extension lengths, and random distributions, with some displaying a lens-like shape that is wider in the center and tapered at both ends (Figure 7I). They are often fully filled with quartz, anhydrite, and fibrous calcite.

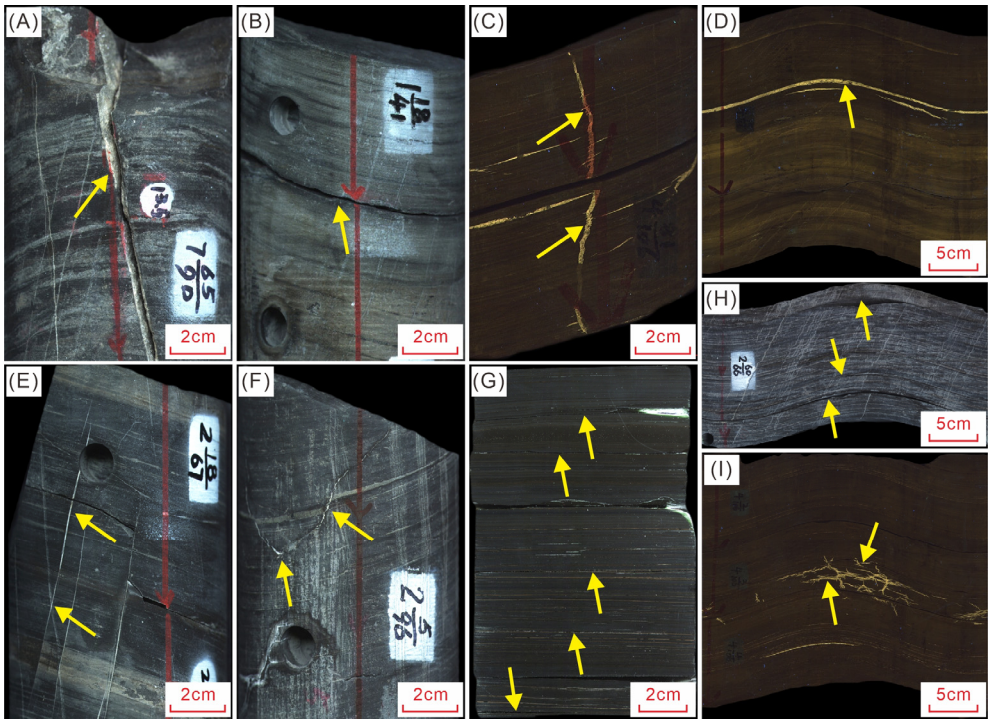

Figure 7. Core photos show natural fractures in upper member of Lower Ganchaigou Formation. (**A**) High-angle unfilled shear fractures, well C12, 3599.58–3599.71 m, external surface of core; (**B**) low-angle unfilled shear fractures, well C13, 3718.19–3718.32 m, external surface of core; (**C**) vertical tensional fractures are filled with anhydrite and calcite, well C908, 2796.78–2796.91 m, external surface fluorescence image of core; (**D**) low-angle shear fractures are filled with anhydrite and calcite, well C908, 2786.50–2786.82 m, circumferential surface fluorescence image of core; (**E**) V-shaped shrinkage fractures are filled with calcite, well C13, 3723.48–3723.61 m, external surface of core; (**F**) dissolution fractures are filled with calcite, well C12, 3530.32–3530.45 m, external surface of core; (**G**) bedding fractures parallel to bedding planes, well C2-4, 2799.50–2799.65 m, longitudinal section of core; (**H**) bedding fractures parallel to bedding planes, well C14, 3847.00–3847.19 m, circumferential surface of core; (**I**) abnormal high-pressure fractures are filled with anhydrite, well C908, 2785.11–2785.39 m, circumferential surface fluorescence image of core.

Image log data provide detailed information about the characteristics of fractures, including dip angle, strike, density and infilling, and so on. Fractures in the study area predominantly appear as sinusoidal patterns in the image logs. High-angle fractures are represented by high-amplitude sinusoidal curves (Figure 8A,B), while low-angle fractures display low-amplitude sinusoidal curves (Figure 8D,E). Horizontal fractures manifest as very low-amplitude sinusoidal curves with minimal width (Figure 8F). Vertical fractures primarily appear as a "geese formation" of double straight lines in the image logs, resembling the characteristics of induced fractures (Figure 8C). Furthermore, due to the fact that fractures in the study area are often filled with high-resistivity minerals such as calcite and anhydrite, filled fractures appear as bright, sinusoidal, and curve-shaped in the image logs (Figure 8A,D) and unfilled fractures appear as dark, sinusoidal, and curve-shaped (Figure 8B,E,F).

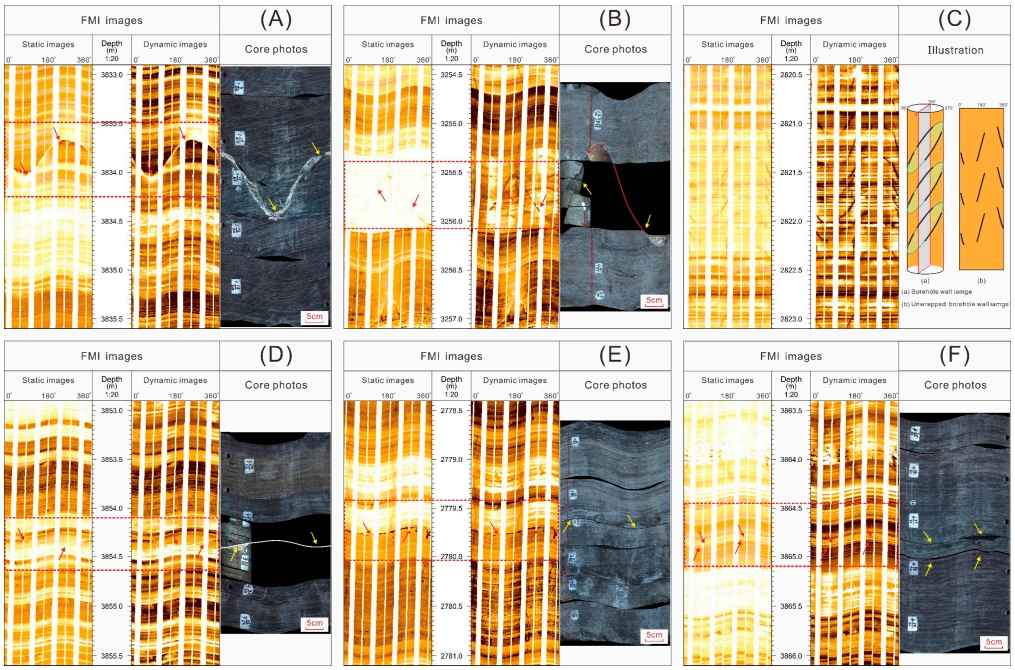

Figure 8. Image log responses of natural fractures in upper member of Lower Ganchaigou Formation of Ganchaigou area. (**A**) Calcite-filled high-angle fractures, well C14; (**B**) high-angle fractures, well C908; (**C**) induced fracture, well C2-4; (**D**) anhydrite-filled low-angle fractures, well C14; (**E**) low-angle fractures, well C908; (**F**) bedding fractures parallel to bedding planes, well C908.

An analysis of core samples and image log data indicates significant variability in the orientation of natural fractures within the study area, with the primary strikes being NNE-SSW and near E-W (Figure 9A). Specifically, conductive fractures (unfilled fractures) predominantly follow the NNE-SSW orientation (marked in red in Figure 9A), while resistive fractures (filled fractures) exhibit two main orientations, namely NNE-SSW and near E-W (marked in green in Figure 9A). The rose diagram of induced fractures shows that their orientation aligns with the NNE-SSW (Figure 9B). According to the principle that the orientation of induced fractures corresponds to the current maximum horizontal principal stress direction [54], this finding suggests that the current maximum horizontal principal stress direction in the study area is NNE-SSW. The dip angles of natural fractures range from 3° to 90°, with the highest concentration between 20° and 30° (Figure 9C). Additionally, calculations of natural fracture parameters reveal that the fracture densities in the study area varies between 0.006 m^{-1} and 5.99 m^{-1}, with an average of 1.91 m^{-1}. Fracture apertures range from 0.008 mm to 1.19 mm, with an average of 0.36 mm.

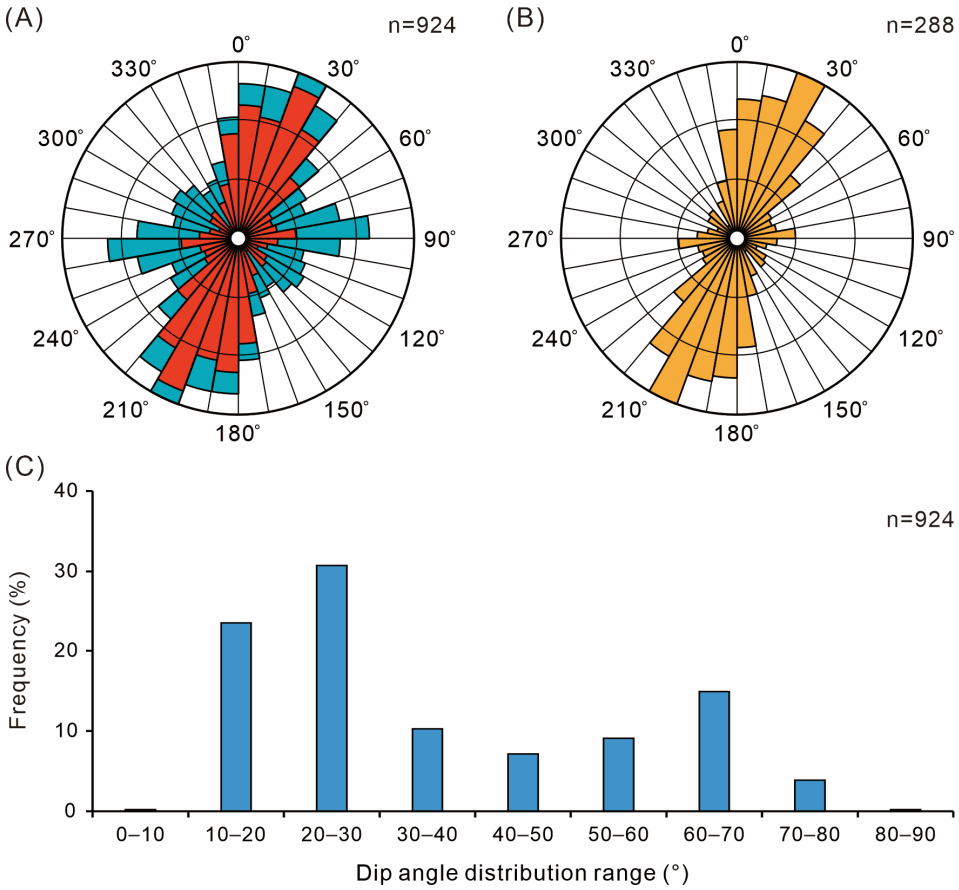

Figure 9. Occurrence parameters of fractures in upper member of Lower Ganchaigou Formation of Ganchaigou area. (**A**) Strike rose diagram of natural fractures derived from core samples and image logs; red represents conductive fractures (unfilled fractures), green represents resistive fractures (filled fractures). (**B**) Strike rose diagram of induced fractures derived from image logs; (**C**) frequency distribution of the dip angle for natural fractures measured from core samples and image logs.

4.2.3. Microscopic Fracture Characteristics

Detailed characteristics of nano-scale to micro-scale fractures were investigated using thin sections and SEM. The results show that a large number of micron-scale fractures have developed in the study area, associated with regional tectonic activity, sedimentary processes, and diagenesis. These fractures represent the microscopic manifestations of tectonic fractures, diagenetic fractures, and abnormal high-pressure fractures.

Tectonic microfractures are formed when rocks undergo one or multiple episodes of stress damage. These fractures often cut through multiple laminae and bending deformation of the laminae and rock fragmentation can be observed around the fracture. The fracture aperture predominantly ranges from 0.005 mm to 1 mm, with considerable variability, and they are frequently filled with pyrite, anhydrite, calcite, or clay minerals (Figure 10A,G). Although the genesis of bedding microfractures is complex, their morphological differences are minor. These fractures are observed along the laminae with good continuity, often circumventing mineral grains and exhibiting a gradual tapering edge. The aperture of these fractures ranges from 10 μm to 200 μm, and they are mostly unfilled, though some are partially filled with calcite (Figure 10B,C). Shrinkage microfractures typically exhibit a regular forward extension at their leading edge, while the trailing edge rapidly tapers in a branched and curved pattern (Figure 10D). These fractures are commonly distributed between mineral grains or crystals, have limited extension distances, and poor continuity (Figure 10H). The aperture of these fractures is mainly between 0.05 μm and 1 μm, and they are often fully filled with calcite (Figure 10D). Dissolution microfractures primarily result from the dissolution of carbonate minerals in an organic acid environment during

organic matter thermal evolution. These fractures are commonly observed between mineral grains and organic matter, featuring highly irregular edges. The aperture ranges from 5 μm to 300 μm, with rapid variation, short extension distances, and low filling degrees, and most of them are unfilled (Figure 10E,I). Microfractures associated with abnormal high pressures generally exhibit a disordered distribution, with noticeable non-directional and highly irregular morphology. They sometimes are mixed with stylolite or occur as bedding microfractures and other fracture types. Their overall extension distance is short, and the filling degree is high, predominantly filled with anhydrite and calcite, making them mostly ineffective fractures (Figure 10F).

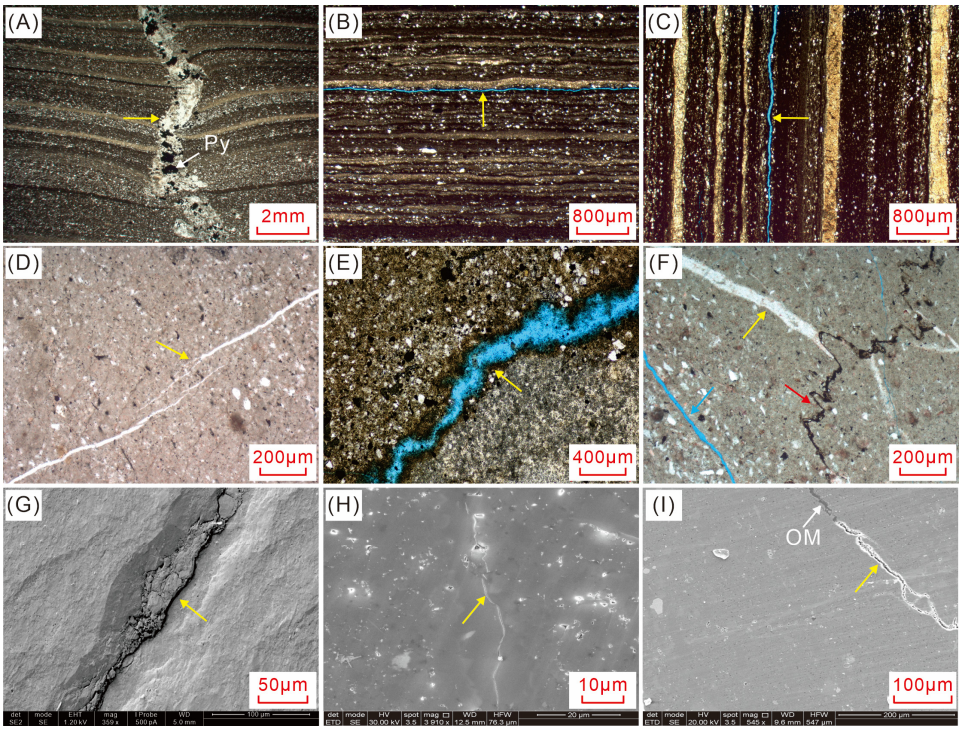

Figure 10. Thin sections and SEM images show natural fractures in upper member of Lower Ganchaigou Formation. (**A**–**F**) Casting thin section images, (**G**) SEM images of freshly broken rock samples, (**H**,**I**) SEM images of argon ion-milled samples. (**A**) Tectonic microfracture is filled with minerals such as anhydrite, calcite, and pyrite (Py), well C12, 3529.90 m, polarized light; (**B**) microfracture parallel to bedding, well C14, 3861.23 m, polarized light; (**C**) microfracture parallel to bedding, well C12, 3609.03 m, vertical section, polarized light; (**D**) shrinkage microfractures are filled with anhydrite and calcite, well C906, 3227.21 m, polarized light; (**E**) dissolution microfractures, well C2-4, 2828.69 m, polarized light; (**F**) abnormal high-pressure fractures (yellow arrow), stylolite (red arrow), and open microfractures (blue arrow), well C2-4, 2818.45 m, polarized light; (**G**) tectonic microfracture, well C2-4, 2822.69 m; (**H**) shrinkage microfracture, well C14, 3842.21 m; (**I**) dissolution microfracture, partially filled with organic matter (OM), well C13, 4216.26 m.

5. Discussion

5.1. Factors Controlling the Fracture Development

Previous studies have demonstrated that the factors governing natural fracture development in shale are complex and diverse, with the dominant factors varying across different regions and different types of shale [15,35,55]. Generally, these factors can be categorized into depositional and diagenetic processes, tectonic processes, and abnormal high-pressure effects. The depositional and diagenetic factors primarily include lithology, mineral composition, lamination structure, rock mechanical properties, bed thickness, organic matter content, and other intrinsic characteristics. These factors are inherent to the rock or originate from its depositional and diagenetic history, serving as the foundational

basis for fracture development. Tectonic processes provide the external load for fracture formation, and their effects can be divided into regional tectonic stress fields and local structural effects [14,22], such as the tectonic position of the rock relative to faults and folds, which is a key factor in explaining the variability of fracture development across different structural settings. Abnormal high-pressure effects, arising from the combined influences of tectonic processes, depositional processes, and diagenetic processes, represent the driving forces for fracture development [53]. Here, we focus on and discuss the six key factors that control the development of fractures in lacustrine mixed shale oil reservoirs, which are mineral composition and brittleness, lamination structure, organic matter content and maturity, diagenesis, tectonic factors, and abnormal high pressure.

5.1.1. Mineral Composition and Brittleness

Mineral composition is a primary factor influencing the mechanical properties of rock, as the inherent characteristics and relative abundance of different minerals can significantly impact rock brittleness, thereby governing fracture development [53,55]. The mineralogical diversity of lacustrine mixed shale oil reservoirs provides favorable conditions for fracture formation.

Cross-plot data reveal a clear positive correlation between carbonate mineral content and the brittleness index (Figure 11A), while felsic mineral content shows a weak negative correlation with the brittleness index (Figure 11B) and clay mineral content exhibits a distinct negative correlation with the brittleness index (Figure 11C). These findings indicate that carbonate minerals contribute most significantly to enhancing rock brittleness in the study area. Moreover, an increase in the brittleness index is accompanied by an increase in fracture density (Figure 11D), suggesting that under equivalent stress conditions, higher rock brittleness leads to a greater degree of fracture development. This phenomenon is primarily attributed to the deviation and branching of the fracture propagation paths when fractures extend into brittle minerals [56]. Further analysis reveals a notable positive correlation between carbonate mineral content and fracture density (Figure 11E). Specifically, increasing dolomite content is associated with a pronounced increase in fracture density, whereas the correlation between calcite content and fracture density is relatively weak (Figure 11F), highlighting the more pronounced positive impact of dolomite on fracture development. No significant correlation is observed between felsic mineral content and fracture density (Figure 11G). Similarly, the contents of quartz and feldspar exhibit no clear relationship with fracture density (Figure 11H), indicating that their influence on fracture development remains uncertain.

5.1.2. Lamination Structure

A lamination structure is a common type of layered structure in sedimentary rocks, typically characterized by abrupt or gradual changes in mineral composition, texture, and color [57]. It significantly affects the physical and mechanical properties of rocks and is closely associated with fracture development. As the fundamental building blocks of a lamination structure, laminae vary in type, density, thickness, and combination styles, which determine the attributes and characteristics of the lamination structure [53,57], thereby controlling fracture development. Three main types of mineral laminae are developed in the shale oil reservoirs of the Ganchaigou area, namely carbonate laminae, clay laminae, and felsic laminae. Statistical analysis shows that the carbonate laminae have the highest fracture density, followed by felsic laminae, with clay laminae showing the lowest fracture density (Figure 12A). Among different mineral laminae combinations, the combinations of carbonate and felsic laminae (C+F) have the highest fracture density, followed by combinations of carbonate, felsic, and clay laminae (C+F+I) and carbonate with clay laminae (C+I), while the combination of clay and felsic laminae (I+F) shows the lowest density (Figure 12B). These findings indicate that carbonate minerals, as the primary brittle minerals in the study area, form laminae and laminae combinations that are more prone to faulting or breakage under stress, thus facilitating fracture development. In contrast,

the laminae and combinations composed of highly plastic clay minerals are generally less brittle, inhibiting fracture development. Felsic laminae and their combinations exhibit intermediate brittleness, having a limited impact on fracture development. Moreover, the presence of different combinations of mineral laminae increases mechanical heterogeneity along the vertical profile [53], resulting in an increase in mechanically weak planes, which enhances the likelihood of laminae fractures under stress, ultimately promoting fracture development.

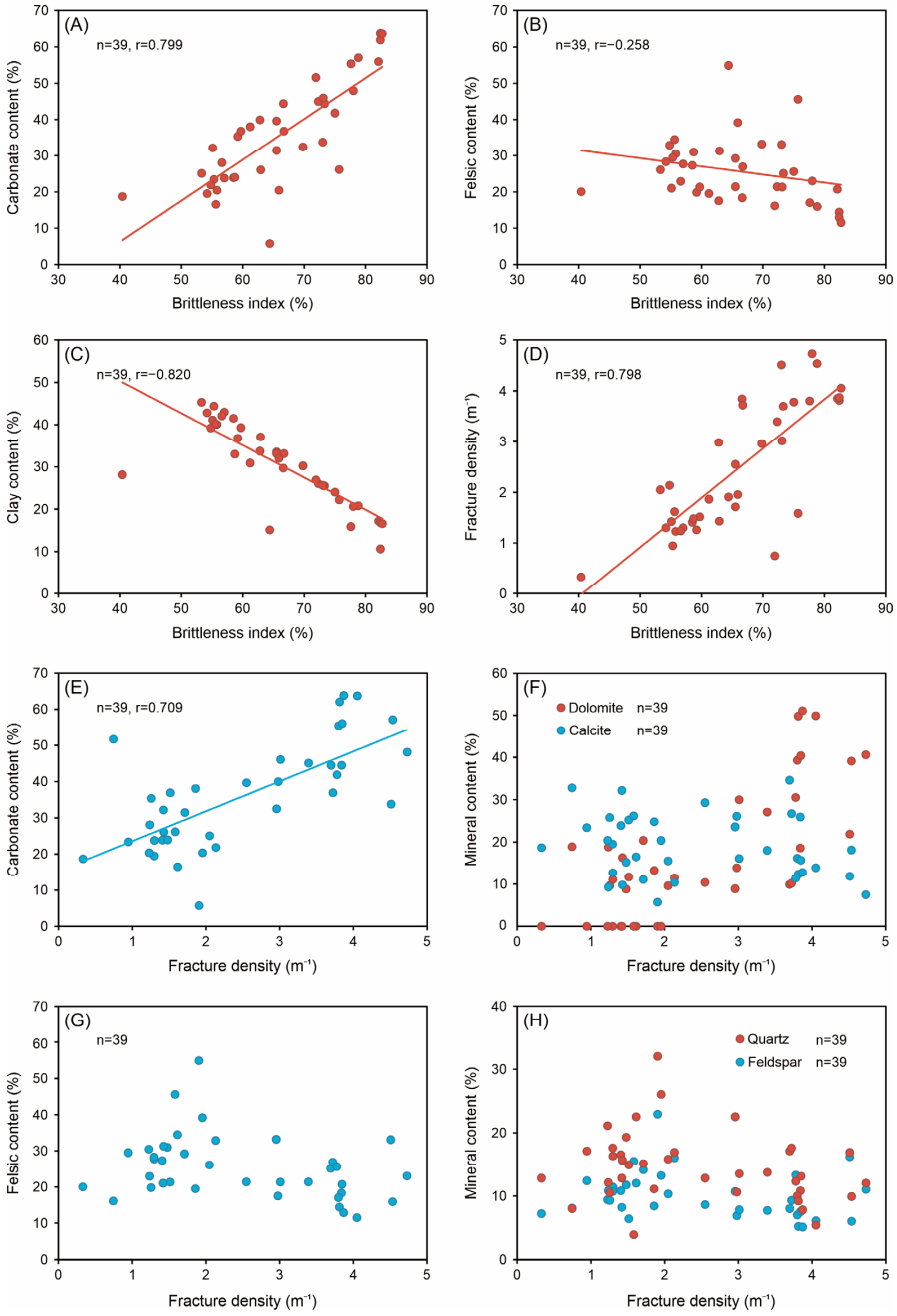

Figure 11. Relationship between fracture density, mineral composition, and rock brittleness. (**A**) Cross-plot of carbonate content versus brittleness index; (**B**) cross-plot of felsic (quartz+feldspar) content versus brittleness index; (**C**) cross-plot of clay content versus brittleness index; (**D**) cross-plot of fracture density versus brittleness index; (**E**) cross-plot of carbonate content versus fracture density; (**F**) cross-plot of dolomite and calcite versus fracture density; (**G**) cross-plot of felsic content versus fracture density; (**H**) cross-plot of quartz and feldspar content versus fracture density. n, number of samples; r, correlation coefficient.

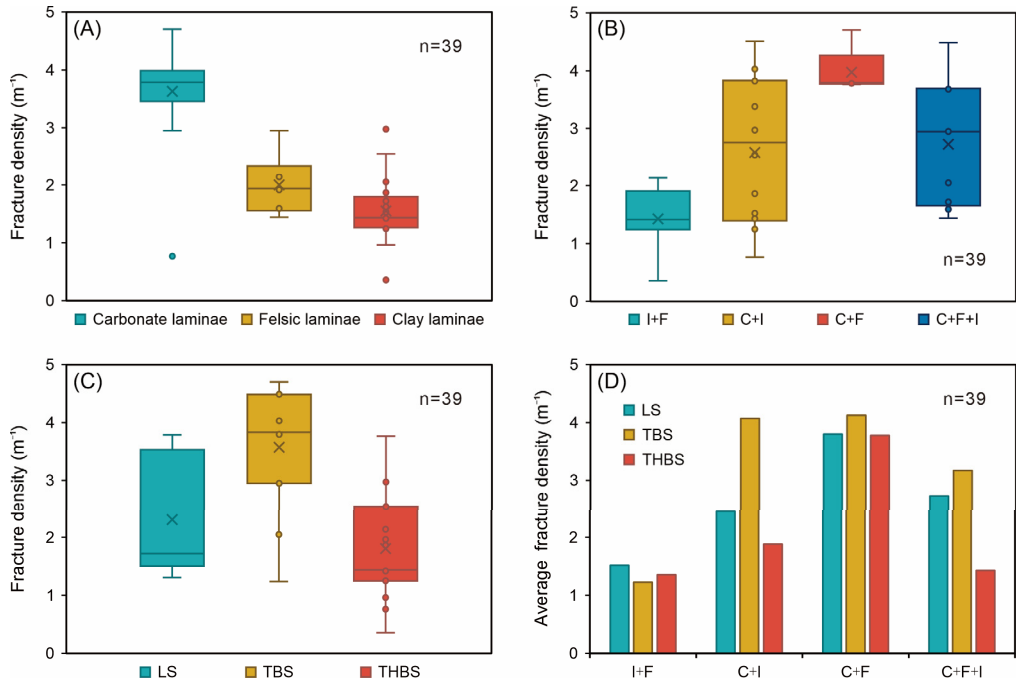

Figure 12. Relationship between lamination structure and fracture development. (**A**) Boxplot showing fracture density of different mineral laminae; (**B**) boxplot showing fracture density of different mineral laminae combinations; (**C**) boxplot showing fracture density of different bedding structures; (**D**) bar chart showing average fracture density of different mineral lamina combinations and bedding structure. I+F, combination of clay laminae and felsic laminae; C+I, combination of carbonate laminae and clay laminae; C+F, combination of carbonate laminae and felsic laminae; C+F+I, combination of carbonate laminae, felsic laminae, and clay laminae; LS, laminated structure; TBS, thin-bedded structure; THBS, thick-bedded structure.

Based on the lamina thickness (LT) and lamina density (LD), lamination structures can be classified into either a laminated structure (LT < 1 cm, LD > 100 m^{-1}), thin-bedded structure (1 cm < LT < 3 cm, 33 m^{-1} < LD < 100 m^{-1}), and thick-bedded structure (3 cm < LT < 10 cm, 1 m^{-1} < LD < 33 m^{-1}). Statistical results indicate that the thin-bedded structure corresponds to the highest fracture density, followed by the laminated structure, while the thick-bedded structure exhibits the lowest fracture density (Figure 12C). An examination of laminae combination styles shows that all combinations, except I+F, conform to the aforementioned trend (Figure 12D). Specifically, thin-bedded structures formed by C+F and C+I combinations reveal the highest average fracture density, followed by C+F+I, with I+F showing the lowest. Laminated structures composed of C+F also exhibit the highest average fracture density, followed by C+F+I and C+I, with I+F remaining the lowest. For thick-bedded structures, C+F shows the highest average fracture density, followed by C+I, while C+F+I and I+F display the lowest densities (Figure 12D).

These results demonstrate that both individual lamina thickness and the density of laminae development are closely related to the degree of fracture development. Within a certain range, as the individual lamina thickness increases and development density decreases, fracture development tends to increase. However, when individual lamina thickness becomes excessively thick and development density is excessively low (thick-bedded structure), stress concentration at fracture tips is inhibited [58], thereby restricting fracture propagation and ultimately limiting fracture development. Conversely, when individual lamina thickness is too thin and development density is extremely high (laminated structure), it often reflects seasonal terrestrial input, which is generally unfavorable for the accumulation of organic matter, thereby inhibiting the development of bedding fractures and reducing fracture density [53]. A comprehensive analysis suggests that the influence of mineral composition on fracture development is relatively more significant

among different lamina combination styles, whereas the impacts of laminae development density and thickness are comparatively less pronounced.

5.1.3. Organic Matter Content and Maturity

The content and maturity of organic matter are closely related to the fracture's development. Statistical results reveal a weak positive correlation between total fracture density and tectonic fracture density with TOC (Figure 13A,B). However, a significant linear positive correlation exists between non-tectonic fracture density and TOC (Figure 13C). Notably, when the TOC exceeds 0.8%, non-tectonic fracture density increases sharply (Figure 13D). Furthermore, statistical data on the Ro and fracture density from 11 core samples in the study area reveal that both total fracture density and non-tectonic fracture density have a distinct linear positive correlation with Ro (Figure 14). These results suggest that organic matter content and maturity significantly control fracture development, with a greater influence on non-tectonic fractures.

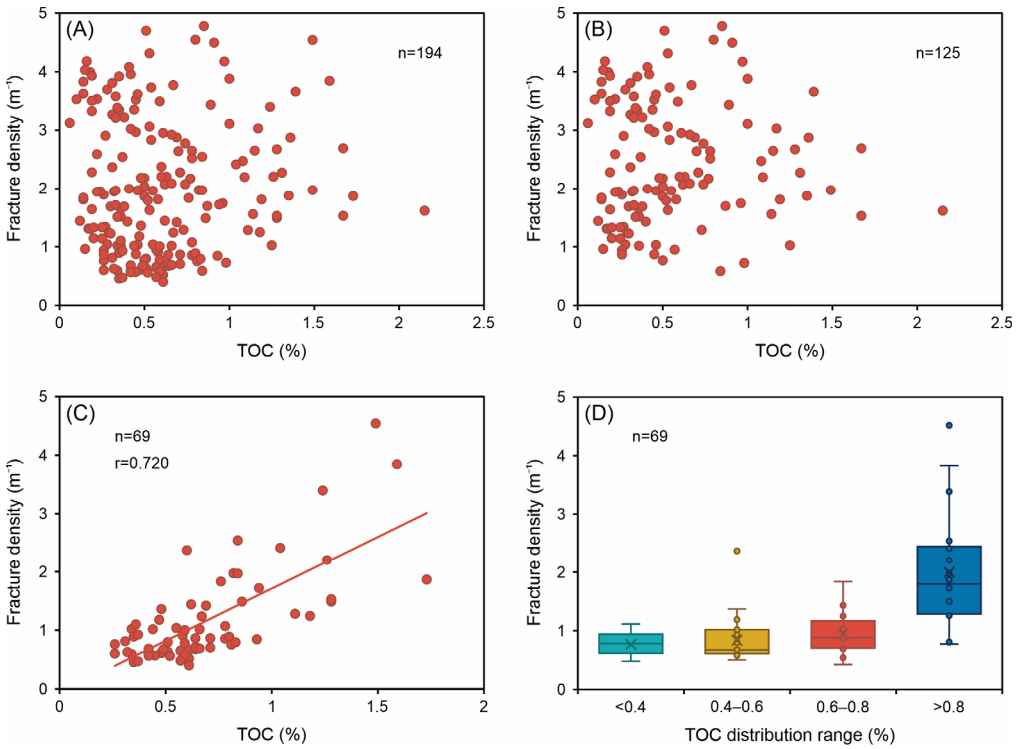

Figure 13. Relationship between organic matter content and fracture development. (**A**) Cross-plot of total fracture density versus total organic carbon (TOC) content; (**B**) cross-plot of tectonic fracture density versus TOC; (**C**) cross-plot of non-tectonic fracture density versus TOC; (**D**) boxplot showing non-tectonic fracture density of different TOC distribution range.

The analysis suggests that the shale strata of the E_3^2 in the Ganchaigou area are characterized by a low TOC and high hydrocarbon generation potential ($S_1 + S_2$), with the thermal evolution of organic matter primarily in the mature stage of oil generation [9]. As organic matter content and thermal maturity increase, the volume of hydrocarbons generated also rises, leading to an increased production of organic acids during hydrocarbon generation. This subsequently causes a rise in localized abnormal fluid pressure [53], which promotes the development of dissolution fractures and bedding fractures, thereby influencing the overall degree of fracture development. Additionally, an increased thermal maturity of organic matter enhances the Young's modulus and hardness of kerogen, resulting in a greater elastic heterogeneity of the rock [59]. This, in turn, further facilitates the formation of bedding fractures.

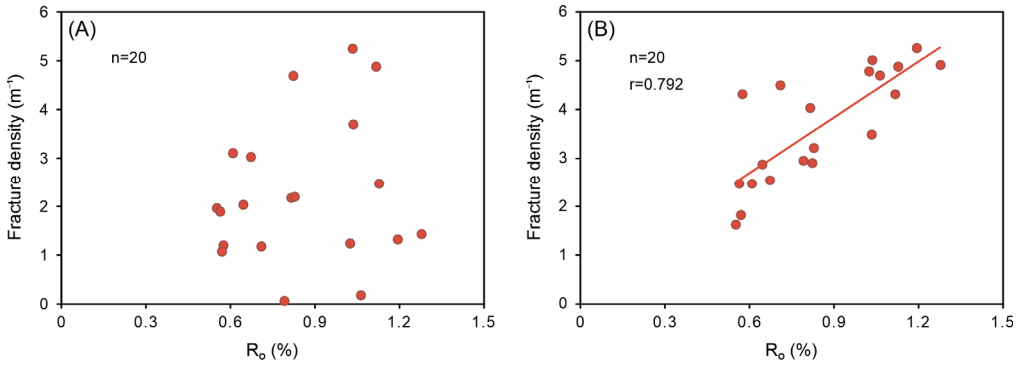

Figure 14. Relationship between organic matter maturity and fracture development. (**A**) Cross-plot of tectonic fracture density versus vitrinite reflectance (Ro); (**B**) cross-plot of non-tectonic density versus Ro.

5.1.4. Diagenesis

Diagenesis significantly influences the development of natural fractures in lacustrine mixed shale oil reservoirs. The formation and evolution of natural fractures are primarily driven by processes such as compaction, dissolution, clay mineral dehydration, and recrystallization in the E_3^2 shale oil reservoirs of the Ganchaigou area. Notably, the shale oil reservoirs in this area are located at depths exceeding 3500 m, meeting the criteria for deep oil and gas reservoirs, with some even classified as ultra-deep [60]. This indicates that the reservoir has undergone intense compaction, which not only increases rock density but also enhances its mechanical strength [14]. Stylolites, frequently observed in thin sections from the study area (Figure 10F), are typically the result of a pressure solution [61]. This evidence further supports the significant role of compaction in controlling the development of natural fractures.

Additionally, the expulsion of hydrocarbons from organic matter releases large quantities of organic acids, which can dissolve minerals such as calcite and dolomite [14]. This dissolution creates pores, some of which may evolve into dissolution fractures (Figure 10E,I). Moreover, the dissolution of minerals or other soluble substances that previously filled fractures can lead to the reopening of these fractures, thereby creating new flow pathways. As hydrocarbon expulsion diminishes and the acidity of formation fluids decreases, dolomite and calcite undergo recrystallization [62], resulting in the formation of intercrystalline pores and shrinkage fractures. The dehydration and transformation of clay minerals comprise another key factor in the development of shrinkage fractures within shale reservoirs [63]. During this process, the release of interlayer water leads to the collapse of interlayers, causing grain volume reduction and the formation of microfractures. In the study area, shrinkage fractures are predominantly found in zones with higher clay mineral content (Figures 7E and 10H), further emphasizing the significant control that clay mineral dehydration exerts on fracture development in lacustrine mixed shale oil reservoirs.

5.1.5. Tectonic Factors

Tectonism is a critical factor controlling the development of tectonic fractures in shale oil reservoirs [19,64]. As previously mentioned, the Yingxiongling structural belt underwent multiple phases of tectonic evolution during the Cenozoic, leading to the formation of compressional folds, compressive shear faults, and other structural features [39]. This tectonic history has resulted in variations in stress distribution across different structural locations [53], leading to significant differences in fracture development. The Ganchaigou block is characterized by a broad and gentle anticline with two primary faults, Ganbei and Gannan, developing in the main area (Figure 1C).

An analysis of cored wells from various locations within the study area reveals a positive correlation between fracture intensity and proximity to these faults. Specifically, tectonic fractures are more pronounced in areas closer to the faults, with fractures in the

hanging wall being notably more developed than those in the footwall (Figure 15A). This finding suggests that areas closer to the faults experience greater tectonic stress, which facilitates fracture formation. When distances to the fault are comparable, the hanging wall, as the more active section, undergoes greater deformation and thus exhibits a higher degree of fracture development than the footwall.

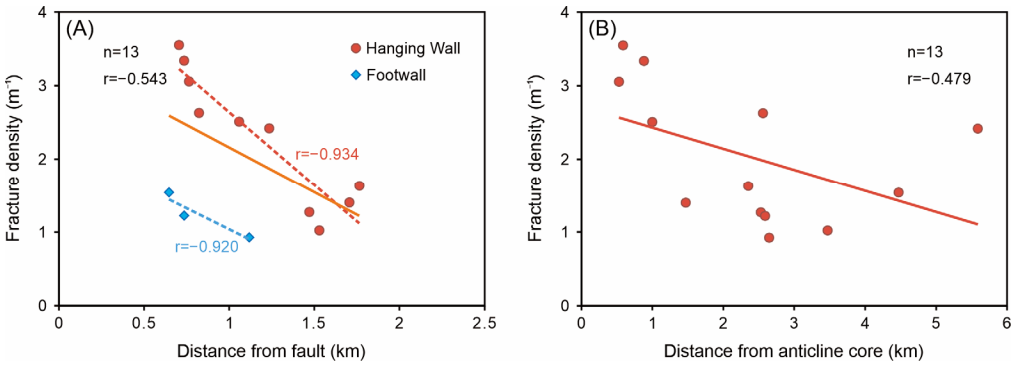

Figure 15. Relationship between tectonic position and fracture development. (**A**) Cross-plot showing density of tectonic fractures at different segments and distances from fault; (**B**) cross-plot showing density of tectonic fractures at different distances from anticline core. Solid line in (**A**,**B**) represents trend line based on statistics of all data points, dashed lines in (**A**) represents trend line based on the corresponding series of data points.

Additionally, previous studies indicate that fold cores with higher stratum curvature are more susceptible to the development of tectonic fractures compared to limbs with lower curvature [53]. Data from the study area reveal a significant negative correlation between fracture density and the distance from the anticline core, with higher fracture densities occurring closer to the core (Figure 15B). This observation indicates that increased tectonic stress concentration leads to more extensive and denser fracture development. These results are consistent with previous research, further affirming the critical influence of tectonic factors on fracture formation and distribution.

5.1.6. Abnormal High Pressure

Abnormal high pressure is a key factor driving the formation of abnormal high pressure fractures and has a significant impact on the development of tectonic fractures and diagenetic fractures. The formation mechanisms of abnormal high pressure in shale oil reservoirs include fault sealing, undercompaction, pressure buildup from organic hydrocarbon generation, and dehydration due to clay mineral transformation [65,66]. These processes indicate that abnormal high pressure can occur at various stages of shale oil reservoir formation. When pore pressure exceeds 1.5 times the hydrostatic pressure, fractures tend to form along mechanically weak surfaces, such as lamination interfaces [67,68]. Furthermore, abnormal high pressure reduces the shear strength of rocks, and once a critical pressure threshold is reached, it can alter the stress state, facilitating the formation and propagation of shear fractures [28].

In the study area, the formation pressure coefficient ranges from 1.3 to 1.8 [9], indicating high formation pressures and abundant formation energy. These high pressures are primarily attributed to the sealing and coverage effects of gypsum–salt layers and the increasing intensity of hydrocarbon generation. During the E_3^2 depositional period, the Ganchaigou area was located in the center of a lacustrine basin, where saline conditions promoted the deposition of extensive gypsum–salt layers [9,69]. These gypsum–salt layers are characterized by dense lithology and strong plasticity, making them less prone to fracturing and providing effective sealing. Additionally, the source rocks in the E_3^1 and the E_3^2 reached their oil generation peaks during the mid-Pliocene to Pleistocene periods (N_2^2–Q) [39]. Consequently, abnormal high pressure is widespread throughout the study area, and abnormal high-pressure fractures are well developed (Figures 7I and 10F). Abnor-

mal high pressure not only promotes the formation of these fractures but also increases pore pressure within the rock, enhancing its tendency to fracture and facilitating the formation of bedding fractures [35]. Moreover, abnormal high pressure promotes fluid flow within the rock, supporting the propagation and connectivity of fractures and increasing the degree of opening in bedding fractures (Figure 10B,C).

5.2. Significance of Fractures for Lacustrine Mixed Shale Oil Reservoirs

5.2.1. Impact of Fractures on Reservoir Space and Seepage Capability

As previously mentioned, the matrix pores in lacustrine mixed shale oil reservoirs exhibit extremely low porosity and permeability, resulting in poor reservoir quality. Under such conditions, the migration and accumulation of shale oil and gas are highly constrained. Therefore, the seepage networks formed by natural fractures of varying types and scales are crucial for facilitating shale oil and gas storage and migration [15,53]. Data from the study area show that the presence of natural fractures significantly improves both reservoir porosity and permeability, with permeability enhancement being especially pronounced (Figure 6). Microfractures connect small-diameter matrix pores, improving pore connectivity and increasing the overall storage capacity (Figure 10). The interconnection of natural fractures of various types and scales forms a seepage network within the shale oil reservoir. Driven by multiple forces, shale oil and gas migrate along the path of least resistance, moving progressively from smaller-scale pore spaces to larger fracture systems, thereby enabling micro-migration. After primary migration, substantial amounts of organic matter and residual hydrocarbons remain within the fracture network, which eventually evolves into a zone of organic matter enrichment, serving as a primary storage space for shale oil and gas. Thus, natural fractures exert a controlling influence on shale oil and gas accumulation by expanding storage space and improving reservoir permeability.

5.2.2. Impact of Fractures on Reservoir Productivity

Previous studies have shown that natural fractures significantly influence oil and gas productivity [16,19,35]. Test and production data from the study area demonstrate that the well sections with high shale oil and gas production are predominantly characterized by the presence of well-developed natural fractures, and there is a clear exponential positive correlation between shale oil and gas production and the degree of natural fracture development (Figure 16).

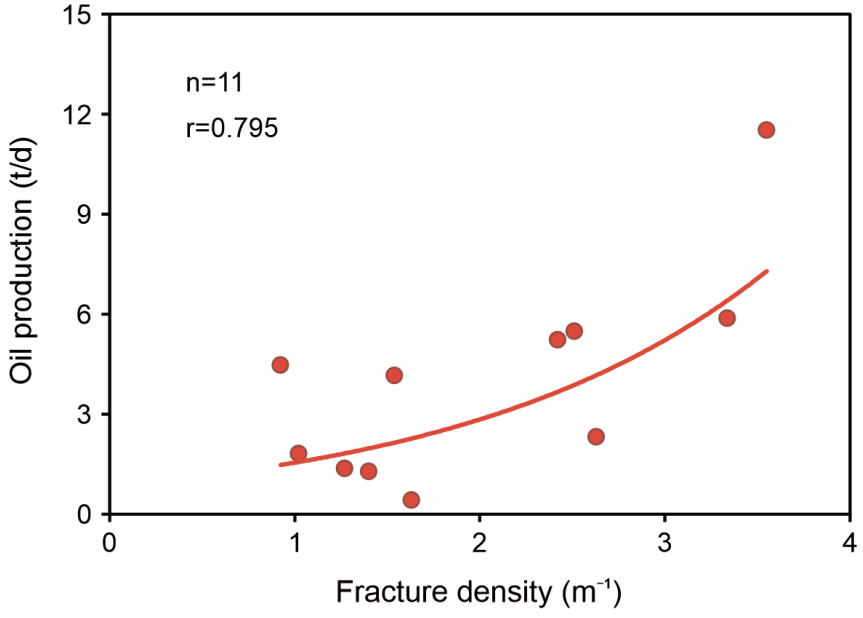

Figure 16. The relationship between oil production and fracture development.

Moreover, in lacustrine mixed shale oil reservoirs, natural fractures not only provide critical storage space and migration pathways for hydrocarbons but also enhance the effectiveness of hydraulic fracturing to a certain extent. When bedding fractures are well developed, hydraulic fractures can more easily connect with natural fractures during propagation, increasing the complexity of the fracture network and significantly improving the effectiveness of volumetric fracturing [20,70]. Consequently, the degree of natural fracture development directly influences the extent of shale oil and gas enrichment and production capacity, making it a key factor in achieving sustained high productivity in mixed shale oil reservoirs.

6. Conclusions

Natural fractures are extensively developed in shale oil reservoirs of the upper member of the Lower Ganchaigou Formation in the Ganchaigou area, Qaidam Basin. Based on geological genesis, these fractures can be categorized into tectonic fractures, diagenetic fractures, and abnormal high-pressure fractures. Tectonic fractures are primarily shear fractures, exhibiting significant variation in dip angles, a wide range of apertures, low development density, and a high filling degree. Diagenetic fractures are predominantly bedding fractures, characterized by low dip angles, small apertures, high development density, and a low filling degree. Abnormal high-pressure fractures display chaotic orientations and complex styles, often consisting of filled fractures. Overall, natural fractures predominantly strike in an NNE-SSW orientation, which is roughly consistent with the current maximum horizontal principal stress direction.

Multiple factors, including mineral composition and brittleness, lamination structures, organic matter content and maturity, diagenesis, tectonic factors, and abnormal high pressure, jointly control the development of fractures in lacustrine mixed shale oil reservoirs. The presence of diverse mineral compositions, a high content of brittle minerals such as dolomite, thin-bedded structures comprising carbonate laminae and felsic laminae, and a high content of mature organic matter provides a favorable foundation for fracture development. Diagenetic processes dominated by dissolution, pressure solution, and mineral dehydration shrinkage, as well as frequent tectonic stresses, ensure favorable conditions for fracture development. Abnormal high pressure, which is the combined product of tectonic, sedimentary, and diagenetic processes, serves as a significant driving force for fracture development.

The lacustrine mixed shale oil reservoirs in the upper member of the Lower Ganchaigou Formation exhibit diverse storage spaces, although the matrix properties are generally poor. The presence of natural fractures significantly enhances pore connectivity and increases storage space. Various types and scales of fractures interconnect, forming an essential seepage network in the shale oil reservoirs. Natural fractures, by influencing the space and seepage capacity of the reservoir, partially control the accumulation and enrichment of shale oil and gas, thereby influencing the degree of enrichment and production capacity. Thus, natural fractures are a critical factor in achieving high and stable production in the lacustrine mixed shale oil reservoirs.

Author Contributions: Conceptualization, X.Z., and G.W.; methodology, X.Z., and G.W.; software, X.Z., and D.L.; validation, D.L., Q.S., and Z.H.; formal analysis, Z.H., Y.L., and K.W.; investigation, J.L., S.W., and D.L.; resources, G.W., Y.S., and K.W.; data curation, Y.L., Y.S., and Q.S.; writing—original draft preparation, X.Z.; writing—review and editing, X.Z., and G.W.; visualization, S.W., and J.L.; supervision, G.W.; funding acquisition, G.W., and S.W. All authors have read and agreed to the published version of the manuscript.

Funding: This research was funded by the National Natural Science Foundation of China, grant number 41872133, and the China Postdoctoral Science Foundation, grant number 2024M753612; GZC20233101.

Data Availability Statement: The data that support the findings of this study are available upon request from the corresponding author, X.Z.

Acknowledgments: We thank PetroChina Qinghai Oilfield Company for providing samples and data access. We are also deeply grateful to the editors and reviewers for their insightful and constructive feedback, which has greatly improved our manuscript.

Conflicts of Interest: Authors Yafeng Li and Kunyu Wu were employed by Qinghai Oilfield Company, CNPC. The remaining authors declare that the research was conducted in the absence of any commercial or financial relationships that could be construed as a potential conflict of interest.

References

1. Schmoker, J.W. Resource-Assessment Perspectives for Unconventional Gas Systems. *AAPG Bull.* **2002**, *86*, 1993–1999.
2. Jarvie, D.M.; Hill, R.J.; Ruble, T.E.; Pollastro, R.M. Unconventional Shale-Gas Systems: The Mississippian Barnett Shale of North-Central Texas as One Model for Thermogenic Shale-Gas Assessment. *AAPG Bull.* **2007**, *91*, 475–499. [CrossRef]
3. Wang, H.; Ma, F.; Tong, X.; Liu, Z.; Zhang, X.; Wu, Z.; Li, D.; Wang, B.; Xie, Y.; Yang, L. Assessment of Global Unconventional Oil and Gas Resources. *Pet. Explor. Dev.* **2016**, *43*, 925–940. [CrossRef]
4. Yang, Z.; Zou, C.; Wu, S.; Lin, S.; Pan, S.; Niu, X.; Men, G.; Tang, Z.; Li, G.; Zhao, J.; et al. Formation, Distribution and Resource Potential of the "Sweet Areas (Sections)" of Continental Shale Oil in China. *Mar. Pet. Geol.* **2019**, *102*, 48–60.
5. Mcmahon, T.P.; Larson, T.E.; Zhang, T.; Shuster, M. Geologic Characteristics, Exploration and Production Progress of Shale Oil and Gas in the United States: An Overview. *Pet. Explor. Dev.* **2024**, *51*, 925–948. [CrossRef]
6. Zou, C.; Zhu, R.; Chen, Z.; Ogg, J.G.; Wu, S.; Dong, D.; Qiu, Z.; Wang, Y.; Wang, L.; Lin, S.; et al. Organic-Matter-Rich Shales of China. *Earth-Sci. Rev.* **2019**, *189*, 51–78. [CrossRef]
7. Zhao, W.; Bian, C.; Li, Y.; Liu, W.; Qin, B.; Pu, X.; Jiang, J.; Liu, S.; Guan, M.; Dong, J.; et al. "Component Flow" Conditions and Its Effects on Enhancing Production of Continental Medium-to-High Maturity Shale Oil. *Pet. Explor. Dev.* **2024**, *51*, 826–838. [CrossRef]
8. Liang, C.; Cao, Y.; Jiang, Z.; Wu, J.; Guoqi, S.; Wang, Y. Shale Oil Potential of Lacustrine Black Shale in the Eocene Dongying Depression: Implications for Geochemistry and Reservoir Characteristics. *AAPG Bull.* **2017**, *101*, 1835–1858. [CrossRef]
9. Li, G.; Zhu, R.; Zhang, Y.; Chen, Y.; Cui, J.; Jiang, Y.; Wu, K.; Sheng, J.; Xian, C.; Liu, H. Geological Characteristics, Evaluation Criteria and Discovery Significance of Paleogene Yingxiongling Shale Oil in Qaidam Basin, NW China. *Pet. Explor. Dev.* **2022**, *49*, 21–36. [CrossRef]
10. Wu, Y.; Liu, C.; Jiang, F.; Hu, T.; Lv, J.; Zhang, C.; Guo, X.; Huang, L.; Hu, M.; Huang, R.; et al. Geological Characteristics and Shale Oil Potential of Alkaline Lacustrine Source Rock in Fengcheng Formation of the Mahu Sag, Junggar Basin, Western China. *J. Pet. Sci. Eng.* **2022**, *216*, 110823. [CrossRef]
11. Liu, B.; Lü, Y.; Meng, Y.; Li, X.; Guo, X.; Ma, Q.; Zhao, W. Petrologic Characteristics and Genetic Model of Lacustrine Lamellar Fine-Grained Rock and Its Significance for Shale Oil Exploration: A Case Study of Permian Lucaogou Formation in Malang Sag, Santanghu Basin, NW China. *Pet. Explor. Dev.* **2015**, *42*, 656–666. [CrossRef]
12. Li, W.; Cao, J.; Shi, C.; Xu, T.; Zhang, H.; Zhang, Y. Shale Oil in Saline Lacustrine Systems: A Perspective of Complex Lithologies of Fine-Grained Rocks. *Mar. Pet. Geol.* **2020**, *116*, 104351. [CrossRef]
13. Jiu, K.; Ding, W.; Huang, W.; Zhang, Y.; Zhao, S.; Hu, L. Fractures of Lacustrine Shale Reservoirs, the Zhanhua Depression in the Bohai Bay Basin, Eastern China. *Mar. Pet. Geol.* **2013**, *48*, 113–123. [CrossRef]
14. Du, X.; Jin, Z.; Zeng, L.; Liu, G.; He, W.; Ostadhassan, M.; Liang, X.; Yang, S.; Lu, G. Characteristics and Controlling Factors of Natural Fractures in Deep Lacustrine Shale Oil Reservoirs of the Permian Fengcheng Formation in the Mahu Sag, Junggar Basin, China. *J. Struct. Geol.* **2023**, *175*, 104923. [CrossRef]
15. Gale, J.F.W.; Laubach, S.E.; Olson, J.E.; Eichhuble, P.; Fall, A. Natural Fractures in Shale: A Review and New Observations. *AAPG Bull.* **2014**, *98*, 2165–2216. [CrossRef]
16. Curtis, J.B. Fractured Shale-Gas Systems. *AAPG Bull.* **2002**, *86*, 1921–1938.
17. Gale, J.F.W.; Reed, R.M.; Holder, J. Natural Fractures in the Barnett Shale and Their Importance for Hydraulic Fracture Treatments. *AAPG Bull.* **2007**, *91*, 603–622. [CrossRef]
18. Zhou, J.; Jin, Y.; Chen, M. Experimental Investigation of Hydraulic Fracturing in Random Naturally Fractured Blocks. *Int. J. Rock Mech. Min. Sci.* **2010**, *47*, 1193–1199. [CrossRef]
19. Ding, W.; Li, C.; Li, C.; Xu, C.; Jiu, K.; Zeng, W.; Wu, L. Fracture Development in Shale and Its Relationship to Gas Accumulation. *Geosci. Front.* **2012**, *3*, 97–105. [CrossRef]
20. Gong, L.; Su, X.; Gao, S.; Fu, X.; Jabbari, H.; Wang, X.; Liu, B.; Yue, W.; Wang, Z.; Gao, A. Characteristics and Formation Mechanism of Natural Fractures in the Tight Gas Sandstones of Jiulongshan Gas Field, China. *J. Pet. Sci. Eng.* **2019**, *175*, 1112–1121. [CrossRef]
21. Shi, J.; Zhao, X.; Pan, R.; Zeng, L.; Luo, W. Natural Fractures in the Deep Sinian Carbonates of the Central Sichuan Basin, China: Implications for Reservoir Quality. *J. Pet. Sci. Eng.* **2022**, *216*, 110829. [CrossRef]
22. Laubach, S.E.; Olson, J.E.; Gross, M.R. Mechanical and Fracture Stratigraphy. *AAPG Bull.* **2009**, *93*, 1413–1426. [CrossRef]
23. Ferrill, D.A.; Morris, A.P.; Hennings, P.H.; Haddad, D.E. Faulting and Fracturing in Shale and Self-Sourced Reservoirs: Introduction. *AAPG Bull.* **2014**, *98*, 2161–2164. [CrossRef]
24. Dashti, R.; Rahimpour-Bonab, H.; Zeinali, M. Fracture and Mechanical Stratigraphy in Naturally Fractured Carbonate Reservoirs-A Case Study from Zagros Region. *Mar. Pet. Geol.* **2018**, *97*, 466–479. [CrossRef]

25. Lai, J.; Wang, G.; Fan, Z.; Wang, Z.; Chen, J.; Zhou, Z.; Wang, S.; Xiao, C. Fracture Detection in Oil-Based Drilling Mud Using a Combination of Borehole Image and Sonic Logs. *Mar. Pet. Geol.* **2017**, *84*, 195–214. [CrossRef]
26. Tabasi, S.; Tehrani, P.S.; Rajabi, M.; Wood, D.A.; Davoodi, S.; Ghorbani, H.; Mohamadian, N.; Alvar, M.A. Optimized Machine Learning Models for Natural Fractures Prediction Using Conventional Well Logs. *Fuel* **2022**, *326*, 124952. [CrossRef]
27. Hui, G.; Chen, Z.; Schultz, R.; Chen, S.; Song, Z.; Zhang, Z.; Song, Y.; Wang, H.; Wang, M.; Gu, F. Intricate Unconventional Fracture Networks Provide Fluid Diffusion Pathways to Reactivate Pre-Existing Faults in Unconventional Reservoirs. *Energy* **2023**, *282*, 128803. [CrossRef]
28. Zeng, L.; Gong, L.; Zhang, Y.; Dong, S.; Lyu, W. A Review of the Genesis, Evolution, and Prediction of Natural Fractures in Deep Tight Sandstones of China. *AAPG Bull.* **2023**, *107*, 1687–1721. [CrossRef]
29. Gong, L.; Fu, X.; Wang, Z.; Gao, S.; Jabbari, H.; Yue, W.; Liu, B. A New Approach for Characterization and Prediction of Natural Fracture Occurrence in Tight Oil Sandstones with Intense Anisotropy. *AAPG Bull.* **2019**, *103*, 1383–1400. [CrossRef]
30. Li, Y.; Chen, X.; Shao, Y. 3D Natural Fracture Model of Shale Reservoir Based on Petrophysical Characterization. *J. Struct. Geol.* **2023**, *166*, 104763. [CrossRef]
31. Zhang, W.; Jian, X.; Fu, L.; Feng, F.; Guan, P. Reservoir Characterization and Hydrocarbon Accumulation in Late Cenozoic Lacustrine Mixed Carbonate-Siliciclastic Fine-Grained Deposits of the Northwestern Qaidam Basin, NW China. *Mar. Pet. Geol.* **2018**, *98*, 675–686. [CrossRef]
32. Liang, C.; Cao, Y.; Wu, J.; Han, Y.; Liu, K.; Hao, F.; Khan, D.; Mei, J.; Zhang, S.; Wang, Y. Water Depth–Terrigenous Input Dynamic Equilibrium Controls the Eocene Lacustrine Shale Laminae Records in Jiyang Depression, Bohai Bay Basin, East China. *AAPG Bull.* **2023**, *107*, 1987–2016. [CrossRef]
33. Cao, Y.; Xi, K.; Niu, X.; Lin, M.; Ma, W.; Zhang, Z.; Hellevang, H. Lamina-Scale Diagenetic Mass Transfer in Lacustrine Organic-Rich Shales and Impacts on Shale Oil Reservoir Formation. *AAPG Bull.* **2024**, *108*, 1327–1356. [CrossRef]
34. Liu, G.; Jin, Z.; Zeng, L.; Huang, L.; Ostadhassan, M.; Du, X.; Lu, G.; Zhang, Y. Natural Fractures in Deep Continental Shale Oil Reservoirs: A Case Study from the Permian Lucaogou Formation in the Eastern Junggar Basin, Northwest China. *J. Struct. Geol.* **2023**, *174*, 104913. [CrossRef]
35. Gong, L.; Wang, J.; Gao, S.; Fu, X.; Liu, B.; Miao, F.; Zhou, X.; Meng, Q. Characterization, Controlling Factors and Evolution of Fracture Effectiveness in Shale Oil Reservoirs. *J. Pet. Sci. Eng.* **2021**, *203*, 108655. [CrossRef]
36. Zhang, C.; Liu, D.; Jiang, Z.; Song, Y.; Luo, Q.; Wang, X. Mechanism for the Formation of Natural Fractures and Their Effects on Shale Oil Accumulation in Junggar Basin, NW China. *Int. J. Coal Geol.* **2022**, *254*, 103973.
37. Fu, S.; Ma, D.; Guo, Z.; Cheng, F. Strike-Slip Superimposed Qaidam Basin and Its Control on Oil and Gas Accumulation, NW China. *Pet. Explor. Dev.* **2015**, *42*, 778–789. [CrossRef]
38. Zhang, D.; Ma, D.; Chen, Y.; Wu, K.; Cai, Z.; Zhao, J.; Wang, J. Research Progress on Oil and Gas Geology and Exploration Practice in Qaidam Basin. *Xinjiang Pet. Geol.* **2019**, *40*, 505–512.
39. Long, G.; Wang, Y.; Zhu, C.; Xia, Z.; Zhao, J.; Tang, P.; Fang, Y.; Li, H.; Zhang, N.; Liu, J. Hydrocarbon accumulation conditions and favorable exploration plays in Yingxiongling structural belt, Qaidam Basin. *Lithol. Reservoirs* **2021**, *33*, 145–160.
40. Fu, S.; Ma, D.; Chen, Y.; Zhang, G.; Wu, K. New advance of petroleum and gas exploration in Qaidam Basin. *Acta Pet. Sin.* **2016**, *37*, 1–10.
41. Guo, D.; Shen, Y.; Lin, H.; Xiong, T.; Zhao, J.; Wang, X.; Wu, K.; Zhao, W.; Xing, H.; Zhang, J.; et al. Post Fracturing Shale Oil Sweet Spot Evaluation in Well CP1 in Yingxiongling Area, Qaidam Basin. *China Pet. Explor.* **2023**, *28*, 117–128.
42. Zhu, C.; Liu, Z.; Song, G.; Long, G.; Gong, Q.; Zhao, J.; Li, S.; Xia, Z.; Wu, Y.; Tian, M. Sedimentary Model, Evolution and Distribution of Paleogene Lacustrine Carbonate Rocks in Yingxiongling Structural Belt, Qaidam Basin. *Acta Pet. Sin.* **2022**, *43*, 1558–1622.
43. Guo, Z.; Sun, P.; Zhang, C.; Tian, J.; Zeng, X. Formation conditions of tight oil & gas and its exploration fields in the Western Qaidam Basin. *Nat. Gas Geosci.* **2014**, *25*, 1366–1377.
44. Guo, Z.; Long, G.; Zhou, F.; Tang, L.; Jiang, Y.; Bai, B.; Zhang, J.; Liu, C.; Wang, Y.; Zhang, B.; et al. Geological characteristics and resource evaluation method for shale oil in a salinized lake basin: A case study from the upper member of the Lower Ganchaigou Formation in western Qaidam depression. *Acta Geol. Sin.* **2023**, *97*, 2425–2444.
45. Xia, Z.; Liu, Z.; Li, S.; Wang, Y.; Wang, P.; Guan, B. Origin and Developing Model of Rock Salt: A Case Study of Lower Ganchaigou Formation of Paleogene in the West of Yingxiong Ridge, Qaidam Basin. *Acta Pet. Sin.* **2017**, *38*, 55–65.
46. *SY/T 5368-2016*; Identification for Thin Section of Rocks. National Energy Administration: Beijing, China, 2016.
47. *SY/T 5162-2021*; Analytical Method of rock Samples by Scanning Electron Microscopy. National Energy Administration: Beijing, China, 2021.
48. *SY/T 5163-2018*; Analysis Method for Clay Minerals and Ordinary Non-Clay Minerals in Sedimentary Rocks by the X-ray Diffraction. National Energy Administration: Beijing, China, 2018.
49. *GB/T 29172-2012*; Practices for Core Analysis. National Standardization Administration: Beijing, China, 2012.
50. *GB/T 19145-2022*; Determination of Total Organic Carbon in Sedimentary Rock. National Standardization Administration: Beijing, China, 2022.
51. *SY/T 5124-2012*; Method of Determining Microscopically the Reflectance of Vitrinite in Sedimentary. National Energy Administration: Beijing, China, 2012.

52. Nelson, R.A. *Geologic Analysis of Naturally Fractured Reservoirs*, 2nd ed.; Gulf Professional Publishing: Houston, TX, USA, 2001; pp. 125–162.
53. Zeng, L.; Lyu, W.; Li, J.; Zhu, L.; Weng, J.; Yue, F.; Zu, K. Natural Fractures and Their Influence on Shale Gas Enrichment in Sichuan Basin, China. *J. Nat. Gas Sci. Eng.* **2016**, *30*, 1–9. [CrossRef]
54. Nian, T.; Wang, G.; Xiao, C.; Zhou, L.; Deng, L.; Li, R. The in Situ Stress Determination from Borehole Image Logs in the Kuqa Depression. *J. Nat. Gas Sci. Eng.* **2016**, *34*, 1077–1084. [CrossRef]
55. Zhang, X.; Shi, W.; Hu, Q.; Zhai, G.; Wang, R.; Xu, X.; Meng, F.; Liu, Y.; Bai, L. Developmental Characteristics and Controlling Factors of Natural Fractures in the Lower Paleozoic Marine Shales of the Upper Yangtze Platform, Southern China. *J. Nat. Gas Sci. Eng.* **2020**, *76*, 103191. [CrossRef]
56. Li, Z.; Li, L.; Li, M.; Zhang, L.; Zhang, Z.; Huang, B.; Tang, C. A Numerical Investigation on the Effects of Rock Brittleness on the Hydraulic Fractures in the Shale Reservoir. *J. Nat. Gas Sci. Eng.* **2018**, *50*, 22–32. [CrossRef]
57. Lazar, O.R.; Bohacs, K.M.; Macquaker, J.H.S.; Schieber, J.; Demko, T.M. Capturing Key Attributes of Fine-Grained Sedimentary Rocks in Outcrops, Cores, and Thin Sections: Nomenclature and Description Guidelines. *J. Sediment. Res.* **2015**, *85*, 230–246. [CrossRef]
58. Zhao, W.; Hou, G.; Zhang, J.; Feng, S.; Ju, W.; You, Y.; Yu, X.; Zhan, Y. Study on the development law of structural fractures of Yanchang Formation in Longdong Area, Ordos Basin. *Acta Sci. Nat. Univ. Pekin.* **2015**, *51*, 1047–1058.
59. Wang, J.; Liu, Y.; Yang, C.; Jiang, W.; Li, Y.; Xiong, Y.; Peng, P. Evolution of Mechanical Properties of Kerogen with Thermal Maturity. *Mar. Pet. Geol.* **2022**, *145*, 105906. [CrossRef]
60. Guo, X.; Hu, Z.; Li, S.; Zheng, L.; Zhu, D.; Liu, J.; Shen, B.; Du, W.; Yu, L.; Liu, Z.; et al. Progress and prospect of natural gas exploration and research in deep and ultra-deep strata. *Pet. Sci. Bull.* **2023**, *8*, 461–474.
61. Toussaint, R.; Aharonov, E.; Koehn, D.; Gratier, J.-P.; Ebner, M.; Baud, P.; Rolland, A.; Renard, F. Stylolites: A Review. *J. Struct. Geol.* **2018**, *114*, 163–195. [CrossRef]
62. Heydari, E.; Wade, W.J. Massive Recrystallization of Low-Mg Calcite at High Temperatures in Hydrocarbon Source Rocks: Implications for Organic Acids as Factors in Diagenesis. *AAPG Bull.* **2002**, *86*, 1285–1303.
63. Metwally, Y.M.; Chesnokov, E.M. Clay Mineral Transformation as a Major Source for Authigenic Quartz in Thermo-Mature Gas Shale. *Appl. Clay Sci.* **2012**, *55*, 138–150. [CrossRef]
64. Griffith, W.A.; Prakash, V. Integrating Field Observations and Fracture Mechanics Models to Constrain Seismic Source Parameters for Ancient Earthquakes. *Geology* **2015**, *43*, 763–766. [CrossRef]
65. Hao, F.; Zou, H.; Gong, Z.; Yang, S.; Zeng, Z. Hierarchies of Overpressure Retardation of Organic Matter Maturation: Case Studies from Petroleum Basins in China. *AAPG Bull.* **2007**, *91*, 1467–1498. [CrossRef]
66. Ma, C.; Elsworth, D.; Dong, C.; Lin, C.; Luan, G.; Chen, B.; Liu, X.; Muhammad, J.M.; Muhammad, A.Z.; Shen, Z.; et al. Controls of Hydrocarbon Generation on the Development of Expulsion Fractures in Organic-Rich Shale: Based on the Paleogene Shahejie Formation in the Jiyang Depression, Bohai Bay Basin, East China. *Mar. Pet. Geol.* **2017**, *86*, 1406–1416. [CrossRef]
67. Kalani, M.; Jahren, J.; Mondol, N.H.; Faleide, J.I. Petrophysical Implications of Source Rock Microfracturing. *Int. J. Coal Geol.* **2015**, *143*, 43–67. [CrossRef]
68. Teixeira, M.G.; Donzé, F.; Renard, F.; Panahi, H.; Papachristos, E.; Scholtès, L. Microfracturing during Primary Migration in Shales. *Tectonophysics* **2017**, *694*, 268–279. [CrossRef]
69. Wan, Y.; Long, G.; Yang, W.; Chai, J.; Ma, X.; Tang, L.; Zhao, J.; Li, H. Hydrocarbon accumulation and evolution characteristics of Paleogene in Yingxiongling area, Qaidam Basin. *Lithol. Reservoirs* **2023**, *35*, 94–102.
70. Xu, D.; Hu, R.; Gao, W.; Xia, J. Effects of Laminated Structure on Hydraulic Fracture Propagation in Shale. *Pet. Explor. Dev.* **2015**, *42*, 573–579. [CrossRef]

Disclaimer/Publisher's Note: The statements, opinions and data contained in all publications are solely those of the individual author(s) and contributor(s) and not of MDPI and/or the editor(s). MDPI and/or the editor(s) disclaim responsibility for any injury to people or property resulting from any ideas, methods, instructions or products referred to in the content.